Chapter 2

Electroweak physics at the Z pole

1 Introduction

With a statistics of Z boson decays five orders of magnitudes, per experiment, higher than LEP, FCC-ee will change the landscape of neutral and charged current precision measurements. As detailed in this chapter, measurements performed at the Z pole by LEP and SLC (Ref. [2]) will see their statistical accuracies improved by up to a statistical factor of 500 – or even more for some quantities dependent on detector performance. In practice this will only be realized if the systematic errors can be improved to the same extent. So far only the most critical of these systematic errors have been discussed for a few quantities: this is the case for the beam energy and energy spread calibration which affects the Z, W and top mass and width measurements as well as the muon pair forward backward asymmetry around the Z peak. There remains a considerable room for further investigations and improvements for many other observables. Nevertheless typical improvements by one to two orders of magnitude seem reasonably within reach, depending on the observable, providing a powerful "electroweak microscope" for physics beyond the standard model.

This Chapter introduces the physics observables accessible at the Z pole, describes the potential of FCC-ee for their precise measurement and gives requirements on luminosity and beam energy determination, on theory calculations, on detector design and experimental uncertainties.

The Chapter is organized as follows. In Section 2 the methods for luminosity measurement are recalled, together with the present theory accuracy and projected precision. In Section 3 measurements of the Z lineshape parameters at FCC-ee, in particular mass and width, are discussed. Section 4 is dedicated to the measurement of the decay widths to specific final states, such as individual lepton species and heavy quarks. The measurement of the invisible width and determination of the number of neutrino families is the subject of Section 5. Accurate measurements of asymmetries at the Z, discussed in Section 6, provide key information for the determination of lepton's and quark's couplings (Section 7). Measurements of $\alpha_{\rm QED}$ and $\alpha_{\rm S}$ are discussed in Section 8 and 2, respectively. The Chapter is concluded by a recall of the detector and accelerator requirements for physics at the Z pole (Section 10),

2 Luminosity measurement

The typical reference process for the luminosity determination at e^+e^- colliders is Bhabha scattering. In particular at LEP small angle Bhabha scattering, with electron/positron scattering angles of the order of few degrees, has been used because, in such kinematical conditions, the contributions to the scattering amplitude due Z-boson exchange diagrams are suppressed with respect to the photon exchange diagrams. As a consequence, small angle Bhabha scattering around the Z peak is essentially a pure QED process, very weakly dependent on Z physics and characterized by a very large cross sections (of the order of 10-100 nb, for typical event selections).

In principle Bhabha scattering cross section can be calculated in QED with very high accuracy. The reference Monte Carlo generator for Bhabha scattering used at LEP was BHLUMI [3–5], whose theoretical formulation is described in detail in Section...[??]. The theoretical uncertainties associated with this code have been thoroughly investigated through independent approaches, thus allowing for a robust estimate of 0.061% of total theoretical uncertainty, at the end of LEP operations. As discussed in Section ...[??], the subsequent progress in the evaluation of light fermion pair corrections as well as in the determination of the running of the QED coupling constant $\alpha(M_Z^2)$ bring current uncertainty at the level of 0.038%. With the present level of accuracy of QED perturbative calculations, together with their matching to resummed higher order corrections, and with an envisaged improvement of a factor of two in the knowledge of $\alpha(M_Z^2)$ before the start of FCC-ee, a total theoretical uncertainty of 0.01% can be realistically achieved (see Tab. C3 of Section....[?].

Experimentally, low-angle Bhabha scattering is measured by detecting two back-to-back electrons on both sides of the apparatus, in a fiducial acceptance corresponding to two annuli defined by radii R_{min} and R_{max}, equivalent to the angular region between the polar angles θ_{min} and θ_{max}, corresponding to the integrated Rutherford cross section

$$\sigma_{bh}^{th} \sim \frac{16\pi\alpha^2}{s}\left(\frac{1}{\theta_{min}^2} - \frac{1}{\theta_{max}^2}\right) .$$

To compute the expected cross section precisely, the fiducial acceptance need to be accurately known, for a typical value of R_{min} around 50 mm and an accuracy in detector position of 10 micron (similar to the accuracy reached at LEP), the systematic error on the luminosity is $\Delta L/L \simeq 2\Delta R_{min}/R_{min} \simeq 4 \cdot 10^{-4}$. Therefore to match the expected improvement in theoretical accuracy for the Bhabha scattering (0.01%) an accuracy in detector position of ≈ 2 microns should be reached, which looks feasible already with present technology. It must be kept in mind that an appropriate choice of the event selection cuts can largely remove the dependence of the luminosity on the relative position between the beams interaction point and the detector, as proposed in [6, 7]. If two different fiducial regions are defined for the two luminosity detectors positioned at the left and right sides with respect to the interaction point, the luminosity measurement can be made independent of transverse misalignments. The dependence on longitudinal misalignments is also largely canceled if the definition of loose and tight is changed from one side to the other side randomly on an event by event basis. In conclusion a precision on the determination of luminosity from low-angle Bhabha scattering of $\approx 0.01\%$ can be expected, both from the theoretical and experimental point of view.

In principle an alternative process, which could allow to overcome the limitation in the precision luminosity determination, is photon pair production $e^+e^- \to \gamma\gamma$. In fact, for this process, the vacuum polarization correction starts to contribute at NNLO level. Moreover, at tree level, photon-pair production is free of Z-exchange diagrams. At present, the theoretical level of knowledge for this process is NLOPS [8], i.e. NLO matched to Leading Logarithmic higher order corrections, which corresponds to a theoretical uncertainty at the 0.1% level. The shortcoming of photon pair production with respect to Bhabha scattering is the lower cross section, in the range of 10-100 pb [9] for large angle event selections, which would require an integrated luminosity of $1.4\ \mathrm{ab}^{-1}$ to reach a statistical error of the order of 0.01%, similar to the one expected for low-angle Bhabha scattering. In addition, photon reconstruction efficiency and rejection against Bhabha scattering events (3 orders of magnitude higher rate) should be carefully analyzed, in order to consider photon pair production as a relevant channel for precision

luminosity determination.

3 The Z lineshape

The scan of the Z resonance provides two parameters playing a key role for the understanding of electroweak interactions: the mass of the Z vector boson and its width. As can be seen from Fig. 2.1 the Z lineshape is considerably distorted by radiation of photons by the electron and positron beams: the production cross section at the peak is strongly reduced and the resonance shape becomes asymmetric, as a result of the shift in effective centre-of-mass energy. The extraction of electroweak parameters from the lineshape requires these ISR QED effects (together with FSR and their interference) to be precisely calculated and kept under control at required precision. It is convenient to define a *radiator function* ($H(s,s')$), which incorporates all ISR corrections, and a *reduced cross section* ($\hat{\sigma}_{f\bar{f}}(s')$) that are convolved in order to compute the visible cross section

$$\sigma_{f\bar{f}}(s) = \int_{4m_f^2}^{s} ds' H(s,s') \hat{\sigma}_{f\bar{f}}(s') \; . \tag{2.1}$$

for all centre-of-mass points included in the energy scan. For LEP data analysis, the radiator function has been computed up to the leading $\mathcal{O}(\alpha^3)$ order [10]. The impact of the uncertainty on ISR corrections to the Z mass and width was computed by comparing two different calculations based either on additive (TOPAZ0) [11, 12] or factorized (ZFITTER) [13, 14] corrections. The precision was found to be of the order of 10^{-5} leading to an uncertainty on the Z mass and width of 100 KeV, which was negligible at LEP, but needs to be improved for FCC-ee with higher order calculations. See Section ...C3, for theoretical isssues related to the QED deconvolution and pseudo-observable definition at FCC-ee.

The $\hat{\sigma}$ reduced cross section, extracted after ISR de-convolution, is composed by three terms

$$\hat{\sigma}_{f\bar{f}}(s) = \sigma_{f\bar{f}}^{peak} \cdot \frac{s\Gamma_Z^2}{\left(s - \mathbf{m}_Z^2\right)^2 + \left(\frac{s\Gamma_Z}{\mathbf{m}_Z}\right)^2} \; + \text{“}(\gamma - Z)\text{”} + \text{“}|\gamma|^2\text{”} \tag{2.2}$$

corresponding to the relativistic Breit-Wigner distribution, to the photon exchange and to the non-factorisable interference term, respectively. While the photon exchange contribution does not depend on m_Z, Γ_Z and therefore poses no problem, the $\gamma - Z$ interference component requires either model dependent assumptions (i.e. assuming the Standard Model form and parameters) or a direct measurement of the cross section off the resonance. The model independent approach follows the so-called S-matrix parametrization [15, 16], where the interference term corresponds to a dimensionless parameter denoted J_{had}^{tot}, whose uncertainty corresponds to a m_Z uncertainty of $\frac{\partial m_Z}{\partial J_{had}^{tot}} = -1.6\ \mathrm{MeV}/0.1$.

At LEP1 the nominal lineshape result was obtained with the model dependent parametrization, because LEP-only data were not sufficient to provide a result with equivalent precision in the S-matrix approach. However, data collected at Tristan at the centre-of-mass energy of about 60 GeV [17], corresponding to an integrated luminosity of 300 pb^{-1} provided a measurement of J_{had}^{tot} with a precision of 0.1, sufficient for a model-independent lineshape-parameters measurement. At FCC-ee a sample of 100 fb^{-1} collected at the centre-of-mass energy of 60 GeV would allow J_{had}^{tot} to be measured with a precision corresponding to an uncertainty on m_Z of

100 keV. Alternatively data collected at higher centre-of-mass energy (i.e. above the Z resonance) could be used to provide a measurement of J^{tot}_{had} of equivalent precision, as shown by the model-independent determination of the Z-mass using LEP2 data [18]. The latter approach is conceptually equivalent, as no Z' resonance has been found up to a few TeV.

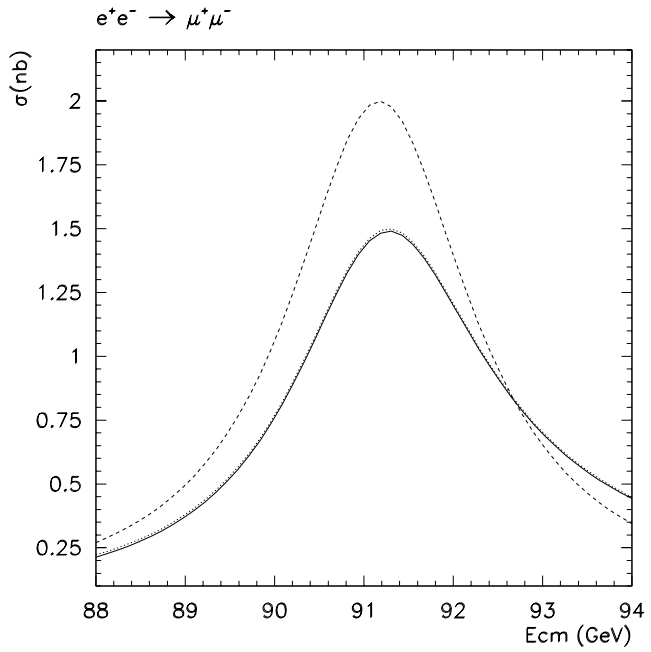

Fig. 2.1: Effect of QED initial state radiative corrections on the muon-pair production cross section near the Z pole. Cross section without initial state radiation (dashed line), $\mathcal{O}(\alpha)$ exponentiated initial state radiation (dotted line), $\mathcal{O}(\alpha^2)$ exponentiated initial state radiation (solid line).

The uncertainty on the m_Z, Γ_Z lineshape parameters is dominated by the knowledge of the centre-of-mass energy at the off-resonance points. At LEP the two off peak points were taken at ± 2 GeV from the Z pole, where sensitivity is maximal and sufficient statistics could be collected, at FCC-ee the choice of the off peak beam energy is driven by requirements linked to the measurement of $\alpha_{\rm QED}(m_{\rm Z}^2)$ described at Section , i.e. at $\approx \pm 3$ GeV from the Z peak. The uncertainty on m_Z and Γ_Z is given approximately by

$$\Delta m_Z \approx 0.5 \Delta (\mathrm{E}_{offpeak-} + \mathrm{E}_{offpeak+}) \tag{2.3}$$

$$\Delta\Gamma_Z \approx \frac{\Gamma_Z}{(\mathrm{E}_{offpeak-} - \mathrm{E}_{offpeak+})}\Delta(\mathrm{E}_{offpeak-} - \mathrm{E}_{offpeak+}) = 0.47\Delta(\mathrm{E}_{offpeak-} - \mathrm{E}_{offpeak+}) \tag{2.4}$$

i.e. the uncertainty on the Z mass (Z width) is given by the correlated (anti-correlated) uncertainty on the centre-of-mass energy at the two off peak points. As described elsewhere in this report, the beam energy is determined with extremely high precision with the technique of resonant depolarization. At LEP the width of the depolarizing resonance was as small as $\approx$ 100 keV, however the beam energy was known with a precision one-order of magnitude worse, because the energy calibration was performed in a few dedicated runs and the related information transported to the events taken during the lineshape scan. At FCC-ee the calibration is foreseen to take place continuously with dedicated non-colliding bunches: as shown in Chapter **??** $\approx$ 100 keV is a realistic goal for the knowledge of the centre-of-mass energy and corresponding uncertainty on m_Z and Γ_Z. This accuracy is obtained for beam energies corresponding to specific recursive values, known as "spin tunes" [19]: the beam energies of the Z and WW threshold scans should be close to half-integer spin tunes. At FCC-ee an half-integer spin tune close to the Z peak is available and corresponds to a centre-of-mass energy of 91.19 GeV. A convenient spin tune value for taking data at about - 3 GeV off peak also exist, corresponding to $\sqrt{s}$ =87.71 GeV. Instead a spin tune value corresponding to peak+3 GeV is not available and the data sample will have to be split between the two closest centre of mass energies, $\sqrt{s}$ =93.85 and 94.73 GeV. These values of the centre-of-mass energies take into account the crossing angle of the two FCC-ee beams (about 30 mrad), giving $\sqrt{s} = 2E_b cos(\alpha/2)$.

The beam energy spread (ϵ_{CMS}) is also affecting the lineshape because it changes the measured cross section by

$$\delta\sigma \simeq 0.5\frac{d^2\sigma}{dE^2}\epsilon^2_{CMS}\,. \tag{2.5}$$

causing a reduction of the visible cross section at peak and an increase of the cross section at the E_{-3}, E_{+3} points, of the order of permil. The net effect on the mass measurement is null, however a correction for the width is required. The size of the energy spread ($\epsilon \approx 60$ MeV) at FCC-ee and its impact on Γ_Z (≈ 4 MeV) is similar to LEP, but the approach to tackle the corresponding systematic uncertainty is different because of the FCC-ee beam crossing angle. At LEP it was controlled at 1% level by measuring the longitudinal size of the beam spot, at FCC-ee can be measured with even better precision from the muon scattering angles in $e^+e^- \rightarrow \mu^+\mu^-(\gamma)$ events. As shown in Ref. [] the crossing angle and the energy of ISR photons can be measured event-by-event and provide distributions sensitive to the beam energy spread. In particular the crossing angle itself can be monitored in real time with very high precision (about 0.01% every 20 s at the Z peak at nominal luminosity) and ISR unfolded with sufficient accuracy using current HO calculations. The corresponding systematic uncertainty on Γ_Z is expected to be less than 30 keV, provided that the muon scattering angles can be measured with an angular resolution of at least 0.1 mrad.

As will be described in next Section, the cross section are measured separately for the Z decay to hadrons and to the three lepton species. The reduced cross sections are then extracted from the data by applying the formalism previously described and the lineshape parameters can be determined in a global fit to the data. In the global fit the decays into charged lepton pairs are incorporated either by introducing in the reduced cross sections the three leptonic partial

widths (Γ_e, Γ_μ and Γ_τ) or by assuming lepton universality: in this case a common leptonic width, Γ_ℓ, is determined. In the latter case four parameters are needed to describe the centre-of-mass dependence of the hadronic and leptonic cross sections: the Z mass (m_Z), the Z width (Γ_Z), the ratio of hadronic to leptonic partial width $R_\ell = \Gamma_h/\Gamma_\ell$ and the hadronic peak cross section σ_h^0. The R_ℓ and σ_h^0 parameters are discussed in next Sections. Table 2.1 gives the dominating uncertainties on the four parameters and the expected precision at FCC-ee. (Note that the statistical uncertainties on the measurements of Z mass and width, as scaled from LEP, are 5 and 8 keV, respectively, for a statistics of 10^12 hadronic Z decays.)

Table 2.1: Dominating sources of systematic uncertainties and expected precision on lineshape parameters from a four parameter fit assuming lepton universality.

Parameter	Dominating source	expected uncertainty	improvement w.r.t. LEP
m_Z	beam energy	100 keV	20
Γ_Z	beam energy	100 keV	20
σ^0_{had}	luminosity	5×10^{-3} nb	20
R_ℓ	exp. acceptance	5×10^{-5}	8

4 Measurement of the normalized Z partial widths

At lepton colliders decays of Z bosons to quarks and charged leptons can be identified with high efficiency and separated from each other and from the small background even with simple criteria, as can be seen from Fig. 2.2 where only charge multiplicity and charged-track momenta are used.

At LEP a simple hadronic selection based on charged track multiplicity and visible energy reached efficiencies higher than 97% in a phase space defined as $\sqrt{\frac{s'}{s}} > 0.10$, while slightly more complex selections based on calorimeters were more than 99% efficient (here s' represents the reduced centre-of-mass energy after ISR). The inefficiency is related to events with most energy lost in the beam pipe region and can be measured from data by rotating real events. Similarly, the small contamination from non resonant two-photon events (indicated as $\gamma\gamma$ in Fig. 2.2) can be estimated from data by counting events with small visible energy as a function of the beam energy (varied during the energy scan), because the non-resonant background is essentially energy independent. Contamination from leptons is relevant only for $\tau^+\tau^-$ events and was kept below 0.5% at LEP. Dominant systematic uncertainties in the selection were due to hadronisation modeling for a charged track selection (typically $\approx 0.05\%$) and knowledge of the detector response for a calorimeter-based selection (typically $\approx 0.10\%$). Both uncertainty can be potentially further reduced at FCC-ee with detailed studies based on data, thanks to the huge statistics.

The selection efficiency of muon pairs in appropriate fiducial regions can be made very high as shown at LEP, where the $\mu^+\mu^-$ selection efficiency was much higher than 99.9% as measured with data using tag-and-probe techniques. The fiducial region can be defined based on the scattering angles in the effective centre-of-mass system, that can be computed by the polar and azimuthal μ^+ and μ^-scattering angles in the lab, $\theta_{\ell^-}, \phi_{\ell^-}$ and $\theta_{\ell^+}, \phi_{\ell^+}$, respectively; at LEP it was possible to cover typically 85% of the phase space with simple cuts. The definition of the acceptance at FCC-ee is slightly complicated by the beam crossing angle α of $\approx$ 30 mrad, giving a boost to the event in the transverse direction, corresponding

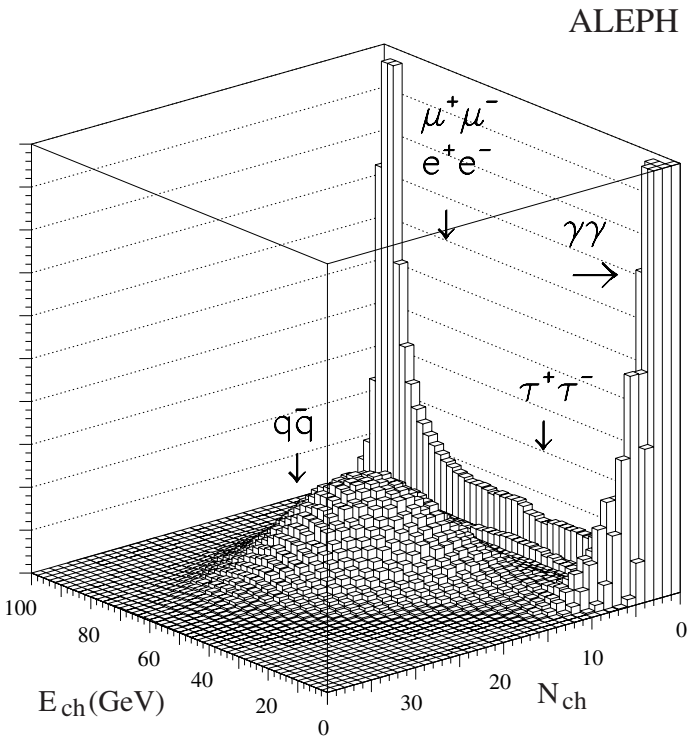

Fig. 2.2: The sum of charged track momenta versus the track multiplicity, for various final states at centre-of-mass energies around the Z peak.

to $\tan\alpha/2 \approx 0.015$. The polar and azimuthal angle in the centre-of-mass system (θ^* and ϕ^*), for a given event are given by $\tan\theta^*\cos\phi^* = \cos\alpha/2(\tan\theta_{\ell^-}\cos\phi_{\ell^-} - \tan\theta_{\ell^+}\cos\phi_{\ell^+})$ and $\cot\phi^* = \cos\alpha/2\frac{\tan\theta_{\ell^-}\cos\phi_{\ell^-} - \tan\theta_{\ell^+}\cos\phi_{\ell^+}}{\tan\theta_{\ell^-}\sin\phi_{\ell^-} + \tan\theta_{\ell^+}\sin\phi_{\ell^+}}$, respectively; ISR modifies further this relation. Dominant systematic uncertainty are related to the knowledge of the acceptance boundaries ($\approx 5\times10^{-4}$ at LEP) and to calorimeter energy resolution in the detection of radiative $\mu^+\mu^-\gamma$ events ($\approx 5\times10^{-4}$ at LEP). Effects related to the muon momentum scale and resolution were already at the $\approx 5\times10^{-5}$ with LEP detectors.

Tau-pair selection is based on low particle multiplicity, narrow jets and the presence of undetected neutrinos. The latter signature can be exploited, e.g., by requiring events with large missing mass. Typical selection efficiencies for $\tau^+\tau^-$ events at LEP were higher than 80% in fiducial regions defined with simple cuts, similar to the muon pair case. For taus systematic uncertainties are dominated by contamination of other Z decays (mostly Bhabha and two-photon events), which can however be monitored with data. At LEP systematic uncertainties at the permil level were obtained. The e^+e^- final state (Bhabha scattering) requires a more complex treatment because of the presence of t-channel production, which can be suppressed by a cut on $\cos\theta^*$. The t-channel subtraction is indeed the dominant source of uncertainty for this channel

($\approx 0.10\%$ at LEP), followed by $\tau^+\tau^-$ background and knowledge of the fiducial acceptance. Improved Monte Carlo calculations, as described in Section 2 have the potential of reducing considerably this uncertainty, compared to LEP times.

In the Z lineshape fit discussed in Section 3 generic hadronic decay selections are treated together with selections of Z decays to individual lepton species and conveniently normalized to cancel the luminosity dependence, giving the ratio of hadronic to leptonic partial width $R_\ell = \sigma_{had}/\sigma_\ell = \Gamma_h/\Gamma_\ell$, where ℓ is a generic charged lepton if lepton universality is imposed. Alternatively R_e, R_μ, R_τ are obtained. At LEP the uncertainty on R_ℓ measurements was dominated by the statistics of leptonic events and therefore a combination of the three lepton species (i.e. assuming universality) provided the best result; at FCC-ee the statistical uncertainty will become neglegible, therefore the best result is expected to come from the muon channel (i.e. from a measurement of R_μ). A measurement of R_μ with a relative precision of 5×10^{-5} is in reach if the systematics related to acceptance are reduced by a factor of ten with respect to LEP. This can be achieved by making measurements independent from the beam spot position and other misalignment effects, for example alternating loose and tight fiducial cuts (similarly to what is done for the luminosity measurement) and by using the high statistics to monitor detector boundaries and efficiencies (tracking uncertainties at LEP were typically of the order of 10^{-4}). In addition the description of ISR and FSR effects ($\mu^+\mu^-\gamma$ events) should be kept at the same level of control. It should be noted that the measurement will take advantage of the increased precision on the beam energy, because $R_\ell = \sigma_{had}/\sigma_\ell$ is strictly a ratio of cross sections at peak and a beam uncertainty of 100 KeV corresponds to a systematic uncertainty of 3×10^{-5}. Another uncertainty, which should be reduced, is the theoretical uncertainty on higher orders, computed at LEP by comparing ZFITTER and TOPAZ0 and corresponding to 2×10^{-4}. In this report a precision of 5×10^{-5} is considered the ultimate precision for R_μ, while for R_τ the need for controlling the e^+e^- and two-photon background suggests a precision goal of 10^{-4}. By taking into account the expected improvements in Monte Carlo simulations used for t-channel substraction a precision of 3×10^{-4} is considered for the R_e measurement.

An efficient selection of Z decays to individual quark flavours is possible only when quark's hadronization products can be efficiently tagged. This is possible for b quarks and, with lower performance, for c quarks. The use of lifetime-based b-quark tagging has been pioneered at LEP, leading to a precise measurement of R_b (with relative precision $\approx 0.3\%$). The presence of two same-flavour quarks in $\mathrm{Z} \to \mathrm{b\bar{b}}$ decays allows the measurement of b tagging efficiency (ϵ_b) directly from data by counting single (N_1^t) and double (N_2^t) tag events by using the relationships

$$N_1^t = 2\,N_{had}\,\left[R_\mathrm{b}\epsilon_b + R_\mathrm{c}\epsilon_c + (1 - R_\mathrm{b} - R_\mathrm{c})\epsilon_{uds}\right]\,, \tag{2.6}$$

$$N_2^t = N_{had}\,\left[R_\mathrm{b}\epsilon_b^2(1+\rho_b) + R_\mathrm{c}\epsilon_c^2 + (1 - R_\mathrm{b} - R_\mathrm{b})\epsilon_{uds}^2\right]\,, \tag{2.7}$$

where ϵ_c and ϵ_{uds} represents the tagging efficiency for c and light quarks, respectively. The ρ_b parameter represents the correlation between the two tags in the same event and it is the most difficult source of systematic uncertainty to be treated (the corresponding uncertainty was $\approx 0.1\%$ at LEP). Sources of correlations are essentially of three kinds: geometrical (e.g. if one b jet is close the the beam pipe, the other tends to be close, too), reconstruction-related (e.g. the same primary vertex used to compute the b-tagging significance for both tags) and related to physics (e.g. momentum correlations between the two b hadrons). The key to control tag correlations is the availability of taggers with high performance (both from the point of

view of detector and software techniques): as an example high tagging efficiency, independent from the b hadron momentum, makes momentum correlations irrelevant. From the pioneering times of LEP, b-taggers have increased their efficiency by a factor three at the same c and light quark contamination level, in the much harsher conditions of LHC. In addition other sources of systematics uncertainties, e.g. related to gluon splitting and to the knowlgedge of ϵ_c, can be studied in details using data already at LHC. Here we consider a factor 3 reduction of the systematic uncertainties on tag correlations largely feasible with modern tracking detectors and taggers, leading to a target precision for $R_{\rm b}$ at FCC-ee of $\approx 0.03\%$.

A pure selection of charm jets is more challenging, however already in the nineties the SLD experiment at SLAC was able to select $\mathrm{Z} \to \mathrm{c\bar{c}}$ decays with a purity of 67% albeit with low efficiency (14%, which would be clearly sufficient at FCC-ee given the large statistics). Charm jets are characterized by the shorter lifetime of charm hadrons, with lower decay multiplicity, and have specific features for specific hadronization and decay modes, for example $D^* \to D^0\pi$, where the soft pion tends to be aligned to the direction of the original charm quark, showing a characteristic peak at $\approx\ 0\ p_T$ with respect to the charm jet axis. Again, the presence of two quarks of the same flavour can be exploited to measure selection efficiency from data; in addition a selection of different decay modes in the two hemispheres (e.g., a specific charm hadron exclusive decay mode on one side and the requirement of inclusive soft pion on the other side) can make two-tag correlations negligible. Here we consider for FCC-ee, an improvement in $R_{\rm c}$ systematic precision with respect to the LEP/SLD measurements of a factor of 3, similar to the b case, leading to an uncertainty on $R_{\rm b}$ at FCC-ee of $\approx 0.15\%$. Selection of Z decays to individual light quark flavours (u, d, s) is not easy, even if low precision measurements were attempted at LEP, e.g. by selecting high momentum strange hadrons. The prerequisite for such measurements is a detailed study of fragmentation properties, with high statistics. We do not give here an estimate of possible precisions for FCC-ee, however the potential for rather precise measurements is certainly concrete.

Table 2.2 gives the statistical an systematic uncertainties on the normalized Z partial widths (R_ℓ) for various final states at FCC-ee, showing also the potential improvement with respect to LEP. **Here we should cite the presently conceivable systematic uncertainties of theoretical origin on partial widths, as contained in the document by Ayres, Sven et al.**

Table 2.2: Relative precision on the normalized Z partial widths (R_f) at FCC-ee (relative uncertainties). Expected statistical and systematic precisions for 150/ab are shown. The last column highligts the improvement on precision with respect to LEP.

	Statistical uncertainty	Systematic uncertainty	improvement w.r.t. LEP
R_μ (R_ℓ)	10^{-6}	5×10^{-5}	25
R_τ	1.5×10^{-6}	10^{-4}	20
$R_{\rm e}$	1.5×10^{-6}	3×10^{-4}	20
$R_{\rm b}$	1.5×10^{-6}	3×10^{-4}	10
$R_{\rm c}$	1.5×10^{-4}	15×10^{-4}	10

5 The Z invisible width and the number of neutrino species

The effect of invisible decays on the Z lineshape is to reduce the peak cross section and increase of the total width of the resonance. A convenient way to determine the Z invisible width is to measure the hadronic cross section at peak, which was the observable used at LEP for the determination of the number of light neutrino families. One of the advantage of the use of the hadronic peak cross section its the very small dependence on other electroweak parameters, such as the top mass, the Higgs mass or the strong-coupling constant, making it an ideal variable to measure Z decays to additional invisible modes or to probe deviations from the Standard Model without the uncertainty related to the lack of knowledge in some of its parameters. The main contribution to the error on the hadronic cross section at peak is given by the theoretical error on the small-angle Bhabha cross section used for the luminosity calculation (Section 2).

The width of the Z to invisible states , Γ_{inv}, can be written as

$$\Gamma_{inv} = \Gamma_Z - \Gamma_h - 3\Gamma_l.$$

The number of light neutrino families N_ν can be obtained from the ratio of the invisible width to the leptonic width, assuming that the invisible width is only due to neutrino final states:

$$\frac{\Gamma_{inv}}{\Gamma_l} = \frac{\Gamma_Z}{\Gamma_l} - R_l - 3 = (\frac{12\pi R_l}{\sigma^0_{had} M_Z^2})^{1/2} - R_l - 3 = N_\nu \cdot \frac{\Gamma_\nu}{\Gamma_l} \tag{2.8}$$

where the dependence on σ^0_{had} has been made explicit. Using the Standard Model prediction for Γ_ν/Γ_l the LEP result was $N_\nu = 2.984 \pm 0.008$ in agreement (within 2 σ !) with the existence of 3 light neutrino families and with a precision dominated by the uncertainty of LEP luminosity. From the expected precision on the small-angle Bhabha scattering cross section discussed in Section 2 and the size of the experimental systematic uncertainties related to the measurement of the instantaneous luminosity, one can estimate that at FCC-ee the number of neutrino families will be determined at the 0.001 level.

The invisible width and the number of light neutrino families can be measured also from the rate of single photon events above the Z peak. These events, showing only a photon of energy

$$E_\gamma = \frac{s - M_Z^2}{2\sqrt{(s)}}$$

in the apparatus, originate from the initial state radiation process $e^+e^- \to \gamma\nu\bar{\nu}$ and their rate is proportional to the number of families. At LEP This direct method gave an uncertainty on the invisible width one order of magnitude larger than the lineshape-based technique, because of the limited statistics on single γ events. At FCC-ee the situation can be potentially reversed, as the statistics collected at and above the WW production threshold is expected to be three orders of magnitudes larger than LEP (Chapter **??**), provided that photon selection and reconstruction efficiencies are kept at per mil level.

6 Measurement of asymmetries

Forward-backward and polarization asymmetries at the Z pole are a powerful experimental tool to investigate quarks and leptons electroweak quantum numbers and to measure the parameter regulating the difference between right-handed and left-handed couplings: the Weinberg

electroweak mixing angle $\sin^2\theta_W$. With unpolarized beam, the amount of Z polarization at production is

$$\mathcal{A}_e = \frac{2g_{Ve}g_{Ae}}{(g_{Ve})^2+(g_{Ae})^2} = \frac{2g_{Ve}/g_{Ae}}{1+(g_{Ve}/g_{Ae})^2}\ . \tag{2.9}$$

The ratio of leptonic couplings is used for the operative definition of the *effective* electroweak mixing angle,

$$\sin^2\theta_{W,eff} \equiv \frac{1}{4}\left(1-\frac{g_{Ve}}{g_{Ae}}\right)\ . \tag{2.10}$$

In the parity violating decay $Z \to f\bar{f}$ the fermion is emitted preferentially in the direction of the Z with an asymmetry coefficient, for fully polarized Z, equal to $\frac{3}{4}\mathcal{A}_f$; for unpolarized beams the resulting forward backward asymmetry is $A_{FB} = \frac{3}{4}\mathcal{A}_e\mathcal{A}_f$.

In the process $e^+e^- \to Z \to f\bar{f}$, for unpolarized beams, the forward-backward asymmetry depends on both initial- and final-state couplings. For leptonic final states A_{FB} shows a quadratic dependence on the electroweak mixing angle ($\approx (1-4\sin^2\theta_{W,eff})^2$), while the dependence is essentially linear for quark final states, resulting in enhanced sensitivity to $\sin^2\theta_{W,eff}$ for quarks, in case of statistically limited measurements. At LEP A_{FB} measurements, for all final states, were limited (by far) by statistical uncertainties, therefore the most precise determination of $\sin^2\theta_{W,eff}$ was coming from b-quark final states and was made assuming the standard model structure for the b couplings. With the huge statistics expected at FCC-ee is possible to follow a different approach, i.e. use leptonic final states for a very precise determination of the electroweak mixing angle, to be used as input to quark forward-backward asymmetries for an independent determination of quark couplings.

From the experimental point of view forward backward asymmetries are robust measurements. In particular it can be shown that by exploiting differential angular distribution the measurement can be made independent of acceptance and angular corrections, provided the selection efficiency is charge- or forward-backward symmetric. The $e^+e^- \to Z \to \mu^+\mu^-$ process is a golden channel for an accurate measurement of A_{FB}; the small experimental systematic uncertainties present at LEP were related to bounds on simultaneous presence of detector and charge asymmetries, whose knowledge was limited only by data statistics, to the $\gamma\gamma \to \mu\mu$ background, which can be made negligible with appropriate cuts (and measured with data) and to the knowledge of the centre-of-mass energy, required to shift the measured asymmetry to the Z pole (m_Z). This last source of uncertainty is expected to yield the dominant systematics at FCC-ee, in spite of one order of magnitude improvement in the beam energy calibration with respect to LEP, described elsewhere in this report. What is relevant for $A_{FB}^{\mu\mu}$ is the relative error between the Z peak point and the two off-peak points, which determine the Z mass. Understanding the point-to-point errors in the energy calibration will be crucial to reduce the corresponding systematic uncertainty. In this report we quote two possible scenarios, in the first case we assume that the knowledge of the point-to-point energy errors will be as good as the one obtained at LEP, in the second scenario we assume very conservatively the entire energy calibration error at the Z peak. The uncertainty on $A_{FB}^{\mu\mu}$ ranges from 8×10^{-6} to 2×10^{-5} , in the two cases, respectively, with a final uncertainty on $\sin^2\theta_{W,eff}$ of $2-5\times10^{-6}$, two order of magnitude better than the uncertainty from leptonic asymmetry obtained at LEP. Large angle Bhabha scattering $e^+e^- \to Z \to e^+e^-$ is also expected to provide information, albeit with reduced sensitivity due to the necessity of t-channel subtraction; the contribution of $e^+e^- \to Z \to \tau^+\tau^-$ is discussed later, in the context of tau polarization measurement.

The measurements of heavy quark forward-backward asymmetries can also be significantly improved at FCC-ee, as LEP results were dominated by statistical uncertainties. The $Z \to b\bar{b}$ forward-backward asymmetry can be measured with two independent techniques, one based on semileptonic b decays and the other on generic selection of b decays with lifetime tagging. The main parameters required for $A_{FB}^{b\bar{b}}$ extraction, such as the χ mixing parameter for semileptonic decays or the hemisphere charge separation for lifetime tagging, can be measured on data, utilizing the same events. The two techniques provided the same sensitivity to $A_{FB}^{b\bar{b}}$ at LEP, and the statistical uncertainty resulting from their combination was a factor of five larger than the most relevant systematic uncertainty, related to QCD corrections, giving room to significant improvements on the measurement of b couplings at FCC-ee. With a six-order of magnitude increase in the statistics of hadronic Z decays, not only the statistical uncertainty will no longer be the dominant uncertainty component, but also detector-related systematics, mostly dependent on studies based on data, will be reduced. The impact of QCD corrections will also be reduced with proper choice of analysis methods (e.g. measure the asymmetry as a function of observables sensitive to gluon radiation), taking advantage of the much higher statistics and, hopefully, with improved QCD calculations. As a simple example based on semileptonic b decays, raising the typical cut on lepton momentum from 3 GeV/c to 10 GeV/c lowers the QCD corrections to 40% of the typical LEP size with a reduction of statistics of a factor for two [20, 21]. Here we conservatively assume that QCD corrections for $Z \to b\bar{b}$ (and $Z \to c\bar{c}$) asymmetries will be reduced by a factor two at FCC-ee. The conservative reduction on detector-related systematic uncertainties is assumed, yielding a total uncertainty on $A_{FB}^{b\bar{b}}$ of 30×10^{-4}, roughly a factor 5 improvement with respect to LEP.

The measurement of $A_{FB}^{c\bar{c}}$ at LEP was based on the selection of semi-exclusive charm decays (e.g. based on D^* mesons) or on semileptonic decays. The modeling of charm decays was the most seizable source of systematic uncertainties, followed by the QCD corrections. The main components of modeling where related to the lepton spectra, the multiplicity of charm decays, the effects related to the presence of $b \to c$ decays. These components are much better known already nowadays for thanks to measurements performed at b factories and will be improved in situ at FCC-ee. A conservative factor of three improvement in the knowledge of charm modeling and the factor of two already mentioned for the QCD corrections uncertainties lead to a a total uncertainty on $A_{FB}^{c\bar{c}}$ of 80×10^{-4}, a factor 4 improvement with respect to LEP.

Production of tau lepton in Z decays, $Z \to \tau^+\tau^-$, represents a special (and extremely useful) case because the polarization of the final-state fermion can be measured through the angular distributions and momenta of the decays products. The tau polarization is defined as

$$P_\tau = \frac{\sigma_R - \sigma_L}{\sigma_R + \sigma_L}, \tag{2.11}$$

its dependence on the polar angle θ can be written as

$$\mathcal{P}_\tau(\cos\theta) = \frac{A_{pol}(1+\cos^2\theta) + \frac{8}{3}A_{pol}^{FB}\cos\theta}{(1+\cos^2\theta) + \frac{8}{3}A_{FB}\cos\theta} \tag{2.12}$$

where $A_{pol} = -\mathcal{A}_\tau$, $A_{pol}^{FB} = -\frac{3}{4}\mathcal{A}_e$ and A_{FB} is as usual related to the product of initial and final state $\mathcal{A}$ factors, showing that a measurement of tau polarization as a function of θ provides a determination of both $\mathcal{A}_\tau$ and $\mathcal{A}_e$ and, consequently, a direct measurement of $\sin^2\theta_{W,eff}$. The statistical uncertainty on both $\mathcal{A}$ factors, dominating at LEP, will be negligible at FCC-ee. The

main systematic uncertainties at LEP were related to the knowledge of tau branching fraction, to tau decay modeling and to higher order electroweak corrections. Improved measurements of tau branching fraction have been made at b factories and can be further improved at FCC-ee, modeling of tau decays can be similarly improved (and could be could be further reduced by using only some of the channels, by trading with statistics): here we have conservatively assumed a factor of three reduction of these uncertainties and a factor of two reduction of theory uncertainties. The resulting uncertainty on $\mathcal{A}_e$ ($\mathcal{A}_\tau$) would be 10×10^{-5} (30×10^{-5}), with an improvement of a factor of 50 (15) with respect to LEP. Note that the dependency on the beam energy is considerably reduced with respect to lepton forward-backward asymmetries, yielding a corresponding systematic uncertainty of only 10^{-5}. The measurement of $\mathcal{A}_e$ yield a determination of $\sin^2\theta_{W,eff}$ of precision similar to the one obtained from $A_{FB}^{\mu\mu}$ (6.6×10^{-6}) without assumption on electron-muon universality. The independent measurement of $\mathcal{A}_e$ can also be used to measure $\mathcal{A}_\mu$ from the muon forward-backward asymmetry.

Table 2.3 gives the statistical an systematic uncertainties on the $\mathcal{A}$ factors for the various final states expected at FCC-ee, showing the potential improvement with respect to LEP.

Table 2.3: Precision on the coupling-ratio factors $\mathcal{A}_f$ for various fermions at FCC-ee. Expected statistical and systematic precisions for 150/ab are shown (relative uncertainties). The last column highligts the improvement on precision with respect to LEP. The last two rows show the expected precision (absolute uncertainties) on $\sin^2\theta_{W,eff}$ from the measurement of the muon FB and tau polarization, respectively.

	Statistical uncertainty	Systematic uncertainty	improvement w.r.t. LEP
$\mathcal{A}_e$	$5. \times 10^{-5}$	$1. \times 10^{-4}$	50
$\mathcal{A}_\mu$	2.5×10^{-5}	1.5×10^{-4}	30
$\mathcal{A}_\tau$	$4. \times 10^{-5}$	$3. \times 10^{-4}$	15
$\mathcal{A}_b$	2×10^{-5}	30×10^{-4}	5
$\mathcal{A}_c$	3×10^{-4}	80×10^{-4}	4
$\sin^2\theta_{W,eff}$ (from muon FB)	10^{-7}	$2 - 5 \times 10^{-6}$	100
$\sin^2\theta_{W,eff}$ (from tau pol)	10^{-7}	6.6×10^{-6}	75

7 Extraction of fermion couplings

The couplings of the neutral current to fermions can be determined using three ingredients:

- the Z partial widths,
- the $\mathcal{A}_f$ parameters as determined by the forward-backward asymmetries and tau polarization,
- the energy dependence of the forward-backward asymmetries.

The partial width of the decay $Z \to f\bar{f}$, gives the sum of the squares of the couplings, while the ratio of the vector and axial couplings is given by the leptonic measurements of $\mathcal{A}_f$, i.e. by the measurement of A_{LR}, of the tau polarisation and of the leptonic forward-backward asymmetries. The energy dependence of the asymmetries fixes the value of the axial couplings, up to a common sign. This last ingredient is required, since the widths and asymmetries do not change if g_v and g_a replace each other.

The expected precision on fermion couplings can be readily computed from the projected uncertainties on on the normalized Z partial widths (R_f) given in Section 4 combined with the projections on A shown in Section 6. The result is shown in Table 2.4. This expected precisions corresponds to an improvement of 1 to 2 orders of magnitudes with respect to LEP.

Table 2.4: Expected precision on fermion axial and vector neutral couplings to the Z (relative uncertainties), computed from the projected uncertainties on on the normalized Z partial widths (R_f) given in Table 2.2 combined with the projections on A shown in Table 2.3.

fermion type	g_a	g_v
e	1.5×10^{-4}	2.5×10^{-4}
μ	2.5×10^{-5}	$2. \times 10^{-4}$
τ	0.5×10^{-4}	3.5×10^{-4}
b	1.5×10^{-3}	1×10^{-2}
c	2×10^{-3}	1×10^{-2}

8 Determination of the electromagnetic coupling constant, $\alpha_{\rm QED}(m_{\rm Z}^2)$

In current electroweak fits, the electromagnetic coupling constant estimated at the Z mass scale, $\alpha_{\rm QED}(m_{\rm Z}^2)$, is estimated with calculations employing dispersion relations for the hadronic contribution to the vacuum polarization. In order to fully exploit the potential of FCC-ee, an improved determination of this "input" standard-model parameters is needed. The measurement of the muon forward-backward asymmetry at the FCC-ee, just below and just above the Z pole, can be used to make a direct determination of $\alpha_{\rm QED}(m_{\rm Z}^2)$ with an accuracy deemed adequate for an optimal use of the FCC-ee precision data.

At a given centre-of-mass energy $\sqrt{s}$, the $\mathrm{e^+e^-} \to \mu^+\mu^-$ production cross section, $\sigma_{\mu\mu}$, is the sum of three terms: the photon-exchange term, $\mathcal{G}$, proportional to $\alpha^2_{\rm QED}(s)$; the Z-exchange term, $\mathcal{Z}$, proportional to G_F^2 (where G_F is the Fermi constant); and the Z-photon interference term, $\mathcal{I}$, proportional to $\alpha_{\rm QED}(s) \times G_F$. The muon forward-backward asymmetry, $A_{\rm FB}^{\mu\mu}$, is maximally dependent on the interference term

$$A_{\rm FB}^{\mu\mu} = A_{\rm FB,0}^{\mu\mu} + \frac{3}{4}\frac{^2}{^2}\frac{\mathcal{I}}{\mathcal{G}+\mathcal{Z}}, \tag{2.13}$$

(where $\mathcal{I} = -0.5$, $\mathcal{J} = \mathcal{I} \times (1 - 4\sin^2\theta_{\rm W}) \simeq -0.037$, and $A^{\mu\mu}_{\rm FB,0} = 3^2a^2/(\mathcal{I}^2 + v^2)^2 \simeq 0.016$ is the small asymmetry at the Z pole), hence varies with $\alpha_{\rm QED}(s)$ as follows:

$$\Delta A^{\mu\mu}_{\rm FB} = \left(A^{\mu\mu}_{\rm FB} - A^{\mu\mu}_{\rm FB,0}\right) \times \frac{\mathcal{Z} - \mathcal{G}}{\mathcal{Z} + \mathcal{G}} \times \frac{\Delta\alpha}{\alpha}. \tag{2.14}$$

This expression shows that the asymmetry is not sensitive to $\alpha_{\rm QED}$ when the Z- and photon-exchange terms are equal, *i.e.*, at $\sqrt{s} = 78$ and $112\,$GeV, where the asymmetry is maximal. Similarly, the sensitivity to the electromagnetic coupling constant vanishes in the immediate vicinity of the Z pole. A maximum of sensitivity is therefore to be expected between $78\,$GeV and the Z pole, on the one hand, and between the Z pole and $112\,$GeV, on the other. With the luminosity targeted at the FCC-ee in one year data taking, the statistical precision expected on $\alpha_{\rm QED}(s)$ is displayed in Fig. 2.3 and indeed exhibit two optimal centre-of-mass energies, $\sqrt{s_-} \simeq 87.9\,$GeV and $\sqrt{s_+} \simeq 94.3\,$GeV. With one year of data at either energy, the expected relative precision on $\alpha_\pm \equiv \alpha_{\rm QED}(s_\pm)$ is of the order of 3×10^{-5}, a factor four smaller than today's accuracy.

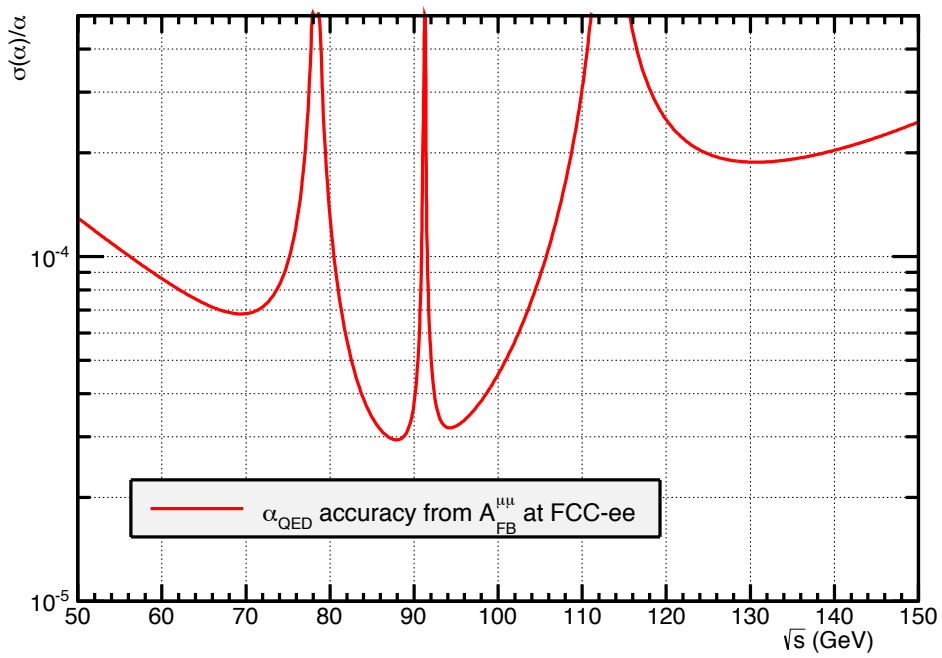

Fig. 2.3: Relative statistical uncertainty for the $\alpha_{\rm QED}(s)$ determination from a measurement of the muon forward-backward asymmetry at the FCC-ee, with a one-year running at any given centre-of-mass energy. The best accuracy is obtained for one year of running either just below or just above the Z pole, at 87.9 and 94.3 GeV, respectively.

A comprehensive list of sources for experimental, parametric, theoretical systematic uncertainties are examined in Ref. [22]. Most of these uncertainties are shown to be under control

Type	Source	Uncertainty
Experimental	$E_{\rm beam}$ calibration	1×10^{-5}
	$E_{\rm beam}$ spread	$< 10^{-7}$
	Acceptance and efficiency	negl.
	Charge inversion	negl.
	Backgrounds	negl.
Parametric	$m_{\rm Z}$ and $\Gamma_{\rm Z}$	1×10^{-6}
	$\sin^2\theta_{\rm W}$	5×10^{-6}
	$G_{\rm F}$	5×10^{-7}
Theoretical	QED (ISR, FSR)	$< 10^{-6}$
	Missing EW higher orders, QED(IFI)	few 10^{-4}
	New physics in the running	0.0
Total (except missing EW higher orders)	Systematics	1.2×10^{-5}
	Statistics	3×10^{-5}

Table 2.5: Summary of relative statistical, experimental, parametric and theoretical uncertainties to the direct determination of the electromagnetic coupling constant at the FCC-ee, with a one-year running period equally shared between centre-of-mass energies of 87.9 and 94.3 GeV, corresponding to an integrated luminosity of $85\,{\rm ab}^{-1}$.

at the level of 10^{-5} or below, as summarized in Table 2.5, often because of the aforementioned delicate cancellation between the two asymmetry measurements. The knowledge of the beam energy, both on- and off-peak, turns out to be the dominant contribution, albeit still well below the targeted statistical power of the method.

The fantastic integrated luminosity and the unique beam-energy determination are *the* key breakthrough advantages of the FCC-ee in the perspective of a precise determination of the electromagnetic coupling constant. Today, the only obstacle towards this measurement stems from the lack of higher orders in the determination of the electroweak corrections to the forward-backward asymmetry prediction in the standard model. With the full one-loop calculation presently available for these corrections, a relative uncertainty on $A_{\rm FB}^{\mu\mu}$ of the order of a few 10^{-4} is estimated. An improvement deemed adequate to match the FCC-ee experimental precision might require a calculation beyond two loops, which may be beyond the current state of the art, but is possibly within reach on the time scale required by the FCC-ee.

9 Determination of the strong coupling constant $\alpha_{\rm S}(m_{\rm Z}^2)$

The rate of hadronic Z decays is very sensitive to the value of the strong coupling constant at the Z mass scale: a precise measurement of R_ℓ is one of the main tools for an accurate determination of $\alpha_s(m_Z^2)$, by assuming the validity of the electroweak theory to compute the ratio of couplings of quarks and leptons to the Z (R_ℓ^{EWK}). One can write

$$R_\ell = R_\ell^{EWK} \times N_C(1 + \sum_{n=1} F_n(\frac{\alpha_s(m_Z^2)}{\pi})^n) \tag{2.15}$$

where N_C is the number of colours and the F_n coefficients are known a at the $\mathcal{O}(\alpha_{\rm S})^4$ [23]. At present, $\alpha_s(m_Z^2)$ is known with a relative precision of 2.3% from LEP data, the jump in

precision for R_ℓ expected at FCC-ee (Section 4) opens the road to a measurement at the 0.2% level. At FCC-ee precise determinations of the strong coupling can also be obtained from W hadronic decays, tau decays and event-shape analyses, as discussed in Chapter **??** *add here pointer to QCD Chapter*.

10 Performance requirements for Z boson physics

10.1 Detector performance requirements

Generally speaking, performance of a modern, general-purpose, e^+e^- detector are adequate for precision physics at the Z pole with FCC-ee. However, there are specific points deserving particular attention in the design of the detector, in order to take full advantage of the physics potential provided by the huge Z decay statistics:

- acceptance effects, related to the knowledge of large-detector boundaries and of tracking efficiency should be given special attention, in order to measure with the required precision leptonic cross sections (e.g.5×10^{-5} for muon pairs). The required level of accuracy is typically one order of magnitude better than for LEP detectors.
- the mechanical stability of luminosity detector should be similarly improved, requiring an accuracy in detector position at the $\approx 2\ \mu m$ level.
- efficient detection of photons and excellent measurement of their energy is important, given the special role of the measurement of tau polarization for couplings. In addition an accurate measurement of low-energy photons ($\approx 1\ GeV$) is relevant to control cuts for radiative events.
- identification of secondary vertexes from B and C hadron decays is very relevant for the measurement of quark couplings. A performance (identification efficiency vs background rejection) similar and better than modern LHC detectors should be the target (a factor 3 better than LEP detectors).

10.2 Specific requirements on the accelerator

The physics reach discussed in this Chapter assumes that 150 ab^{-1} are delivered by the accelerator (100 ab^{-1} at peak, the rest at off-peak points). The other important requirement is the an accurate calibration of the beam energy, an order of magnitude better than LEP. The robustness of this assumption is discussed in detail in Chapter **??** *pointer to the transverse polarization section*. It should be reminded that knowledge of the centre-of-mass energy affects not only the determination of the mass and width of the Z boson, but also other key observables, as asymmetries and cross section ratios. Another accelerator parameter, which play an important role is the beam energy spread, however its size and stability can be efficiently monitored with data (dimuon events).

Chapter 3

Di-boson physics

1 Introduction

To be done by Fulvio and Roberto after the rest

A detailed account of the di-boson physics studied at LEP is given in Ref. [24], together with the dominant sources of systematic uncertainties.

Di-boson production at FCC-ee includes $\mathrm{e^+e^-} \to \mathrm{W^+W^-}, \mathrm{ZZ}, \mathrm{Z}\gamma$ or $\gamma\gamma$ processes. The large luminosities at and above the WW threshold and up to $\sqrt{s} \sim 370$ GeV will deliver large samples of di-boson and even tri-boson events. (Give numbers.)

These large statistics enable the measurements of many electroweak parameters with unprecedented accuracies. Among these measurements are the mass and the width of the W boson, m_{W} and Γ_{W}, the trilinear and quadrilinear gauge couplings, the number of neutrino species, the strong coupling constant, or the centre-of-mass energy. The pertaining experimental strategy is outlined, and the FCC-ee potential summarized.

Give the outline of the chapter, as well as the objectives (requirements on luminosity measurement, centre-of-mass energy and energy spread measurement, detector designs, theory calculations, experimental uncertainties ...)

2 Measurement of the W mass and width at the WW threshold

The W mass is a fundamental parameter of the standard model (SM) of particle physics, currently measured with a precision of 15 MeV [25], from the combination of Tevatron and LEP2 determinations. In the context of precision electroweak precision tests the W mass direct measurement uncertainty is currently limiting the sensitivity to possible effects of new physics [26], as indirect constraints place more stringent limits of the W mass value.

A precise direct determination of the W mass can be achieved by observing the rapid rise of the W-pair production cross section near its kinematic threshold around 161 GeV. The advantages of this method are that it only involves selecting and counting events, it is clean and uses all decay channels.

W mass measurement at a single energy point

In 1996 the LEP2 collider delivered $\mathrm{e^+e^-}$ collisions at a single energy point near 161 GeV, with a total integrated luminosity of about 10 pb^{-1} at each of the four interaction points. The data was used to measure the W-pair cross section (σ_{WW}) at 161 GeV, and extract the W mass with a precision of 200 MeV [27–30].

Taking data at a single energy point the statistical sensitivity to the W mass with a simple event counting is given by

$$\Delta m_{\mathrm{W}}(\mathrm{stat}) = \left(\frac{d\sigma_{\mathrm{WW}}}{dm_{\mathrm{W}}}\right)^{-1} \frac{\sqrt{\sigma_{\mathrm{WW}}}}{\sqrt{\mathcal{L}}} \frac{1}{\sqrt{\epsilon p}} \tag{3.1}$$

where $\mathcal{L}$ is the data integrated luminosity, ϵ the event selection efficiency and p the selection purity. The purity can be also expressed as

$$p = \frac{\epsilon\sigma_{\mathrm{WW}}}{\epsilon\sigma_{\mathrm{WW}} + \sigma_B}$$

where σ_B is the total selected background cross section.

A systematic uncertainty on the background cross section will propagate to the W mass uncertainty as

$$\Delta m_{\mathrm{W}}(B) = \left(\frac{d\sigma_{\mathrm{WW}}}{dm_{\mathrm{W}}}\right)^{-1} \frac{\Delta\sigma_B}{\epsilon}. \tag{3.2}$$

Other systematic uncertainties as on the acceptance ($\Delta\epsilon$) and luminosity ($\Delta\mathcal{L}$) will propagate as

$$\Delta m_{\mathrm{W}}(\mathrm{A}) = \sigma_{\mathrm{WW}} \left(\frac{d\sigma_{\mathrm{WW}}}{dm_{\mathrm{W}}}\right)^{-1} \left(\frac{\Delta\epsilon}{\epsilon} \oplus \frac{\Delta\mathcal{L}}{\mathcal{L}}\right), \tag{3.3}$$

while theoretical uncertainties on the cross section ($\Delta d\sigma_{\mathrm{WW}}$) propagate directly as

$$\Delta m_{\mathrm{W}}(\mathrm{T}) = \left(\frac{d\sigma_{\mathrm{WW}}}{dm_{\mathrm{W}}}\right)^{-1} \Delta\sigma_{\mathrm{WW}}(\mathrm{T}). \tag{3.4}$$

Finally the uncertainty on the center of mass energy E_{CM} will propagate to the W mass uncertainty as

$$\Delta m_{\mathrm{W}}(\mathrm{E}) = \left(\frac{d\sigma_{\mathrm{WW}}}{dm_{\mathrm{W}}}\right)^{-1} \left(\frac{d\sigma_{\mathrm{WW}}}{dE_{\mathrm{CM}}}\right) \Delta E_{\mathrm{CM}}, \tag{3.5}$$

that can be shown to be limited as $\Delta m_{\mathrm{W}}(\mathrm{E}) \leq \Delta E_{\mathrm{CM}}/2$, and in fact for E_{CM} near the threshold it is $\Delta m_{\mathrm{W}}(\mathrm{E}) \simeq \Delta E_{\mathrm{CM}}/2$, so it is the beam energy uncertainty that propagates directly to the W mass uncertainty.

In the case of $\mathcal{L} = 8$ ab^{-1} accumulated by the FCCee data taking in one year, and assuming the LEP event selection quality [27] with $\sigma_B = 300$ fb and $\epsilon = 0.75$, a statistical precision of $\Delta m_{\mathrm{W}} \simeq 0.35$ MeV is achievable if the systematic uncertainties will not be limiting the precision, i.e. if the following conditions are achieved:

$$\Delta\sigma_B < 0.6 \text{ fb} \tag{3.6}$$

$$\left(\frac{\Delta\epsilon}{\epsilon} \oplus \frac{\Delta\mathcal{L}}{\mathcal{L}}\right) < 2 \cdot 10^{-4} \tag{3.7}$$

$$\Delta\sigma_{\mathrm{WW}}(\mathrm{T}) < 0.8 \text{ fb} \tag{3.8}$$

$$\Delta E_{\mathrm{CM}} < 0.35 \text{ MeV} \tag{3.9}$$

corresponding to precision levels of $2 \cdot 10^{-3}$ on the background, $2 \cdot 10^{-4}$ on acceptance and luminosity, $2 \cdot 10^{-4}$ on the theoretical cross section, and $4 \cdot 10^{-6}$ on the beam energy.

W mass and width measurements at two or more energy points

In the SM the W width is well constrained by the W mass, and the Fermi constant, with a $\sim \alpha_S/\pi$ QCD correction due to the hadronic decay contributions; the W width is currently measured to a precision of 42 MeV [25]. The first calculations of the W boson width effects in $\mathrm{e^+e^-} \to \mathrm{W^+W^-}$ reactions have been performed in Ref. [31], and revealed the substantial effects

of the width on the full cross section lineshape, in particular at energies below the nominal threshold.

From the determination of σ_{WW} at a minimum of two energy points near the kinematic threshold both the W mass and width can be extracted [32].

In the following the YFSWW3 version 1.18 [33] program has been used to calculate σ_{WW} as a function of the energy (E_{CM}), W mass (m_{W}) and width (Γ_{W}). Figure 3.1 shows the W-pair cross section as a function of the $\mathrm{e^+e^-}$ collision energy with W mass and width values set at the PDG [25] average measured central values $m_{\mathrm{W}} = 80.385$ GeV and $\Gamma_{\mathrm{W}} = 2.085$ GeV, and with large 1 GeV variation bands of the mass and width central values.

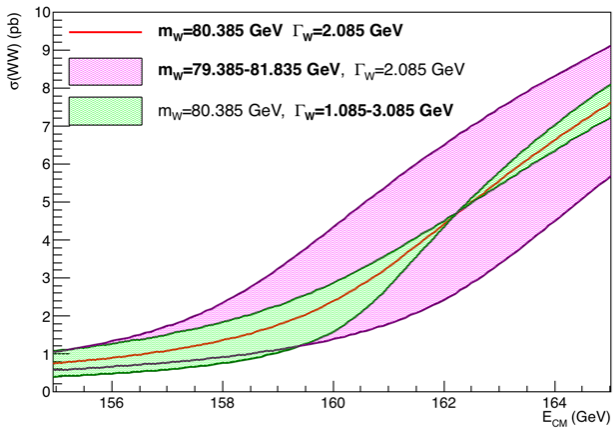

Fig. 3.1: W-pair production cross section as a function of the $\mathrm{e^+e^-}$ collision energy E_{CM} as evaluated with YFSWW3 1.18 [33]. The central curve corresponds to the predictions obtained with $m_{\mathrm{W}} = 80.385$ GeV and $\Gamma_{\mathrm{W}} = 2.085$ GeV. Purple and green bands show the cross section curves obtained varying the W mass and width by ± 1 GeV.

It can be noted that while a variation of the W mass roughly corresponds to a shift of the cross section lineshape along the energy axis, a variation of the W width has the effect of changing the slope of cross section lineshape rise. It can also be noted that the W width dependence shows a crossing point at $E_{\mathrm{CM}} \simeq 2m_{\mathrm{W}} + 1.5\mathrm{GeV} \simeq 162.3$ GeV, where the cross section is insensitive to the W width.

Figures 3.2 and 3.3 show the differential functions relevant to the statistical and systematical uncertainties for a measurement of the W mass and width from the W-pair cross section near the kinematic threshold, similarly as discussed for the single energy point W mass extraction. For the statistical terms the efficiency and purities are evaluated assuming an event selection quality with $\sigma_B \simeq 300$ fb and $\epsilon \simeq 0.75$.

The minima of the mass differential curves plotted in Fig. 3.2 indicate the optimal points to take data for a W mass measurement, in particular minimum statistical uncertainty is achieved with $E_{\mathrm{CM}} \simeq 2m_{\mathrm{W}} + 0.6$ GeV$\simeq 161.4$ GeV. The minima of the width differential curves, on Fig. 3.3, indicate maximum sensitivity to the W width, while all curves diverge at the W width insensitive point $E_{\mathrm{CM}} \simeq 162.3$ GeV, where $d\sigma_{\mathrm{WW}}/d\Gamma_{\mathrm{W}} = 0$.

If two cross section measurements $\sigma_{1,2}$ are performed at two energy points $E_{1,2}$, both the W mass and width can be extracted with a fit to the cross section lineshape. The uncertainty

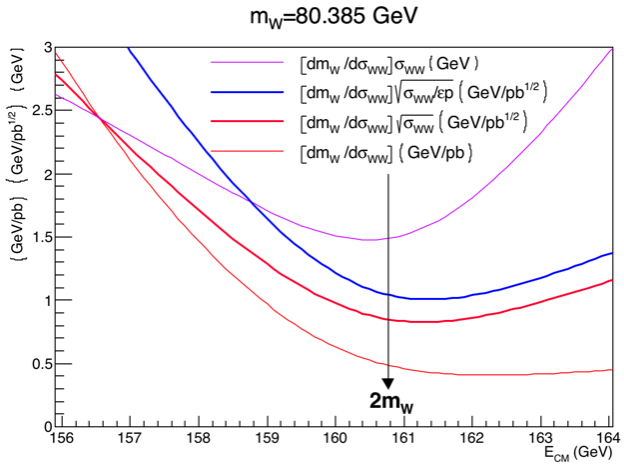

Fig. 3.2: W-pair cross section differential functions with respect to the W mass, evaluated with YFSWW3 1.18 [33]. The central mass value is set to $m_{\mathrm{W}} = 80.385$ GeV.

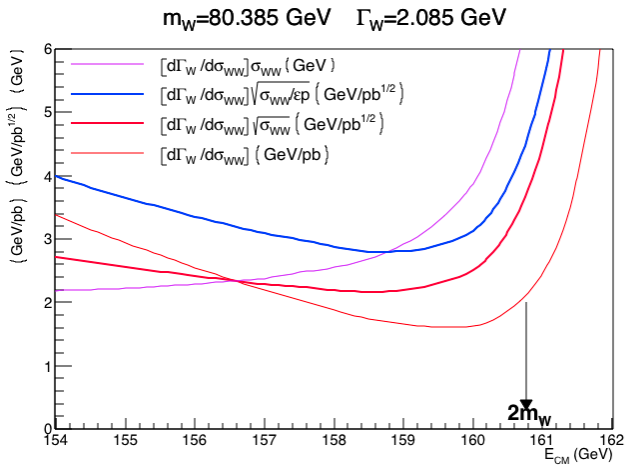

Fig. 3.3: W-pair cross section differential functions with respect to the W width, evaluated with YFSWW3 1.18 [33]. Central mass and width values are set to $m_{\mathrm{W}} = 80.385$ GeV and $\Gamma_{\mathrm{W}} = 2.085$ GeV.

propagation would then follow

$$\Delta\sigma_1 = \frac{d\sigma_1}{dm}\Delta m + \frac{d\sigma_1}{d\Gamma}\Delta\Gamma = a_1\Delta m + b_1\Delta\Gamma \tag{3.10}$$

$$\Delta\sigma_2 = \frac{d\sigma_2}{dm}\Delta m + \frac{d\sigma_2}{d\Gamma}\Delta\Gamma = a_2\Delta m + b_2\Delta\Gamma. \tag{3.11}$$

The resulting uncertainty on the W mass and width would be

$$\Delta m = -\frac{b_2\Delta\sigma_1 - b_1\Delta\sigma_2}{a_2 b_1 - a_1 b_2} \tag{3.12}$$

$$\Delta\Gamma = \frac{a_2\Delta\sigma_1 - a_1\Delta\sigma_2}{a_2 b_1 - a_1 b_2} \tag{3.13}$$

If the $\Delta\sigma_{1,2}$ uncertainties on the cross section measurements are uncorrelated, e.g. only statistical, the linear correlation between the derived mass and width uncertainties is

$$r(\Delta m, \Delta\Gamma) = \frac{1}{\Delta m \Delta\Gamma} \frac{a_2 b_2 \Delta\sigma_1^2 + a_1 b_1 \Delta\sigma_2^2}{(a_2 b_1 - a_1 b_2)^2} \tag{3.14}$$

Optimal data taking configurations

When conceiving data taking at two different energy points near the W-pair threshold in order to extract both m_{W} and Γ_{W}, it is useful to figure out which energy points values E_1 and E_2, would be optimally suited to obtain the best measurements, also as a function of the data luminosity fraction f delivered at the higher energy point. For this a full 3-dimensional scan of possible E_1 and E_2 values, with 10 MeV steps, and of f values, with 0.05 steps, has been performed, and the data taking configurations that minimize arbitrary combination of the expected statistical uncertainties on the mass and the width $F(\Delta m_{\mathrm{W}}, \Delta\Gamma_{\mathrm{W}})$ are found.

For example, in order to minimize the simple sum of the statistical uncertainties $F(\Delta m_{\mathrm{W}}, \Delta\Gamma_{\mathrm{W}}) = \Delta m_{\mathrm{W}} + \Delta\Gamma_{\mathrm{W}}$, the optimal data taking configuration would be with

$$E_1 = 157.10\ \mathrm{GeV}, \qquad E_2 = 162.34\ \mathrm{GeV}, \qquad f = 0.40. \tag{3.15}$$

With this configuration, and assuming a total luminosity of $\mathcal{L} = 8\ \mathrm{ab}^{-1}$, the projected statistical uncertainties would be

$$\Delta m_{\mathrm{W}} = 0.60\ \mathrm{MeV} \qquad \text{and} \quad \Delta\Gamma_{\mathrm{W}} = 1.50\ \mathrm{MeV}. \tag{3.16}$$

With this same data taking configuration,the statistical uncertainty obtained when measuring only the W mass would yield $\Delta m_{\mathrm{W}} = 0.55$ MeV, just slightly better with respect to the two-parameter fit. On the other hand the $\Delta m_{\mathrm{W}} = 0.55$ MeV precision obtained in this way must be compared with the $\Delta m_{\mathrm{W}} = 0.35$ MeV statistical precision obtainable when taking all data at the most optimal single energy point $E_0 = 161.4$ GeV.

When varying the $F(\Delta m_{\mathrm{W}}, \Delta\Gamma_{\mathrm{W}})$ target to optimize towards, the obtained optimal energy points don't change much, with the upper energy always at the Γ_{W}-independent $E_2 = 162.34$ GeV point, and the optimal lower E_1 point at $(1-2)\Gamma_{\mathrm{W}}$ units below the nominal $2m_{\mathrm{W}}$ threshold, $E_1 = 2m_{\mathrm{W}} - (1-2)\Gamma_{\mathrm{W}}$, according to if the desired precision is more or less focused on the W mass or the W width measurement. In a similar way the optimal data fraction to be taken at the lower off-shell E_2 energy point varies according to the chosen precision targets, with larger fractions more to the benefit of the W width precision. When a small fraction of data (e.g. f =0.05) is taken off-shell a statistical precision $\Delta m_{\mathrm{W}} = 0.39$ MeV is recovered both in the single- (m_{W}) and the two-parameter ($m_{\mathrm{W}}, \Gamma_{\mathrm{W}}$) fits.

Considering that the beam energies E_b that can surely be calibrated with resonant depolarization are such that the spin tune is a half integer, that is

$$E_b = 0.4406486(\nu + 0.5) \quad \mathrm{GeV} \tag{3.17}$$

where ν is and integer, the scan of energy points can be limited to a grid with $E_{\mathrm{CM}} = 0.8812972(\nu + 0.5) \quad \mathrm{GeV}$. Taking this grid constraint into account the optimal higher energy point for data taking becomes the $E_2 = 162.62$ GeV for $\nu = 184$. The corresponding optimal statistical precisions attainable are increased by 5-10% with respect to the velues reported above. For the case of minimizing $\Delta m_{\mathrm{W}} + \Delta\Gamma_{\mathrm{W}}$, would be with taking data with $E_1 = 157.33$ GeV,$E_2 = 162.62$ GeV, $f = 0.40$ and yielding statistical uncertainties $\Delta m_{\mathrm{W}} = 0.65$ MeV and $\Delta\Gamma_{\mathrm{W}} = 1.59$ MeV assuming a total integrated luminosity $\mathcal{L} = 8\ \mathrm{ab}^{-1}$.

Data taking at additional energy points

In the case of limiting correlated systematics uncertainties, it can be useful to take data and measure both signal and background cross section at more than two $E_{\rm CM}$ points, in order to reduce background and acceptance uncertainties.

In particular, for the simultaneous measurement of $m_{\rm W}$ and $\Gamma_{\rm W}$ just described, taking data at energy points where the differential factors $(d\sigma/dm_{\rm W})^{-1}$, $(d\sigma/d\Gamma_{\rm W})^{-1}$, $\sigma(d\sigma/dm_{\rm W})^{-1}$ and $\sigma(d\sigma/d\Gamma_{\rm W})^{-1}$, are equal, can help cancelling the effect of correlated systematic uncertainties of background and acceptance.

Measuring the W-pair cross section at additional points can also serve to disentagle other possible new physics effects at threshold; for example measuring the $\beta_{\rm W}^3$ raise of the triple gauge coupling (TGC) cancellation effects.

3 Measurement of W decay couplings

With the full FCC-ee physics program, a total of around 130M W-pair events will be produced, with a majority at the $\sqrt{s}$= 240 GeV energy. As the LEP2 program has demonstrated, a very large fraction of the produced W-pair events can be collected (85-95% efficiency), with low background levels (90-95% purity), in all decay final states, including fully hadronic qqqq, semi-leptonic $\ell\nu$qq, and fully leptonic $\ell\nu\ell\nu$ channels, with $\ell = {\rm e}$, μ and τ.

The event yields in the qqqq channel, the three $\ell\nu$qq channels, and the six $\ell\nu\ell\nu$ channels can be combined, taking into account their cross-contaminations and correlations, in order to fit the W decay branching ratios, and the total W-pair cross sections. A fit that does not assume W-lepton coupling universality can be performed to extract the leptonic decay couplings $B{\rm e}$, $B\mu$ and B_τ, while a fit that assumes lepton universality can be performed to extract the hadronic decay coupling Bq. In both fits the sum of leptonic and hadronic branching fractions is constrained to unity.

Final results of these two fits making use of LEP2 data [24, 34] are shown in Fig. 3.4. The results without lepton universality revealed an excess of tau decays with respect to both the electron and muon decay channels. This excess has been quantified to be at the level of 2.6 standard deviations significance, by making use of the ratio $2B_\tau/(B{\rm e} + B\mu)$.

It will be very difficult to confirm or rule out this tau channel excess by making use of W decays in the LHC data, due to systematic uncertainty limitations with identifying tau decays in high energy hadron collisions. Only a future collider like the FCCee, that can deliver a very large, comprehensive and clear collection of 10^8 W boson decays, will certainly be able to provide a clarification on this tau discrepancy.

Table 3.1: Relative precision on the determination of the W decay branching ratios. Final combined results with LEP2 data are compared to the projected precision obtainable with FCC-ee.

Decay mode relative precision	$B(\mathrm{W} \to \mathrm{e}\nu)$	$B(\mathrm{W} \to \mu\nu)$	$B(\mathrm{W} \to \tau\nu)$	$B(\mathrm{W} \to qq)$
LEP2	1.5%	1.4%	1.8%	0.4%
FCC-ee	$3{\cdot}10^{-4}$	$3{\cdot}10^{-4}$	$4{\cdot}10^{-4}$	$1{\cdot}10^{-4}$

Projected precisions on the W boson decays to hadrons, e μ and tau leptons achievable

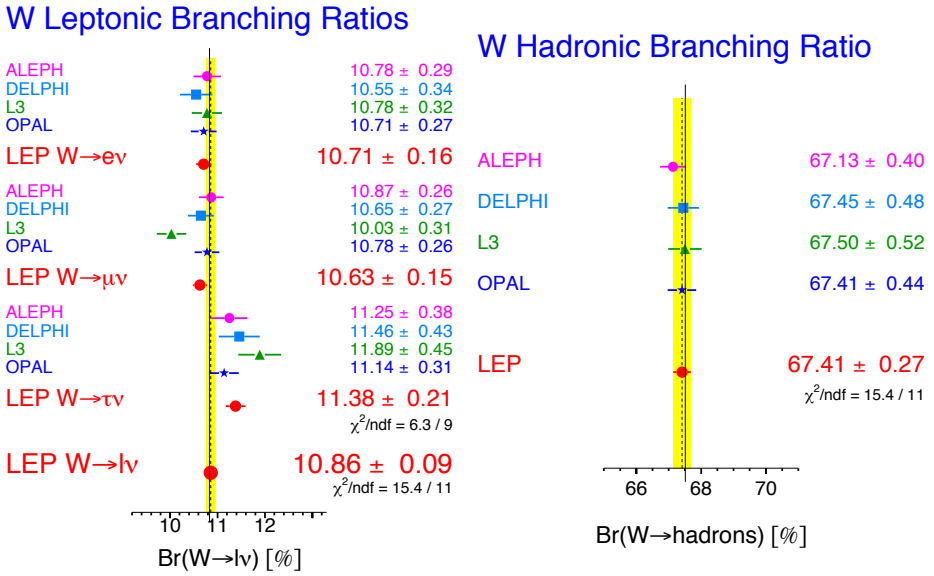

Fig. 3.4: Leptonic W decay branching ratios (left) and hadronic W decay branching ratio assuming lepton-flavor universality (right) as currently determined by LEP2 data [24]

with the FCCee program are shown in Table 3.1, and compared to LEP2 precisions. In these projections the impact of systematic uncertainties on the FCC-ee precisions will be comparable but not much larger than the statistical uncertainty. This will be achievable by using data-driven methods on independent data, to constrain the leading systematics, e.g. using tag and probe methods to measure the selection performances of jet reconstruction and lepton identification. The estimated improvement of the FCC-ee precision with respect to existing LEP2 results ranges from ~ 30 for the hadronic decays, to ~ 50 for muon decays.

Within the Standard Model the W boson hadronic branching ratio B_q is related to the Cabibbo-Kobayashi-Maskawa (CKM) quark mixing matrix, and to the strong coupling constant α_S through the relation

$$R_W = \frac{B_q}{1-B_q} = 3\left(1+\frac{\alpha_S(m_W^2)}{\pi}\right)\sum_{i=u,c;j=d,s,b}|V_{ij}|^2. \tag{3.18}$$

As discussed also in section 2, assuming CKM unitarity with $S_W = \sum_{i=u,c;j=d,s,b}|V_{ij}|^2 = 2$, the B_q determination can be used to extract the value of $\alpha_S(m_W^2)$. Focusing on fitting directly the R_W ratio of hadronic to leptonic decay rates, the projected achievable $\alpha_S(m_W^2)$ relative precision is 0.2% [35].

If the CKM unitarity is not assumed in the sum, and $\alpha_S(m_W^2)$ is taken form other independent precision determinations, the B_q and R_W measurements can be used in turn to provide a stringent test of CKM unitarity for the five lightest quarks S_W at the precision level of few 10^{-4}. The determination of S_W can in turn be employed to derive the value of the least well determined CKM element $|V_{cs}|$, with a precision bounded by the uncertainty on the sum of the other five elements in S_W.

The flavour tagging of jets from W decays can be exploited to perform more direct mea-

surements of $|V_{cs}|$ and of the overall fraction of W boson decays to charm quarks R_c [36–38]. The final achievable statistical precision on R_c will be at the 10^{-3} level, or better.

The FCC-ee data will also allow to explore the more rare W $\rightarrow$bc and bu events, where respectively $\sim 10^5$ and $\sim 10^3$ decays are expected from a total of 200M W boson decays. Also in the case of W boson jet-flavour determinations we expect that dominant systematic uncertainties, related to jet-tagging performances, will be data-driven and constrained by the collected luminosity. These measurements will lead to direct determinations of the $|V_{cb}|$ and $|V_{ub}|$ CKM matrix elements with precisions better than 1% for $|V_{cb}|$ and around 5% for $|V_{ub}|$, therefore improving the knowledge of the quark-mixing matrix. Such measurements were not fully exploitable at LEP2 given the low statistics of collected W decays.

Any other rare decay of the W boson can be explored with FCC-ee data with a sensitivity that can probe the level of 10^{-7} decay probabilities. In this context particular interest will be in measuring exclusive radiative decays [39] that will provide stringent tests of the QCD factorization formalism and enable novel searches for new physics. Other exclusive rare hadronic decays [40, 41] will also be accessible with FCC-ee data.

4 Kinematic determination of the W mass and width

In addition to the W mass and width measurements achievable through the W-pair cross sections near the production energy threshold described in Sec. 2, the W mass and width can also be determined from the kinematic reconstruction of the W-pair decay products. This was the primary method to measure the W mass and width with LEP2 data [24], leading to the results shown in Fig 3.5.

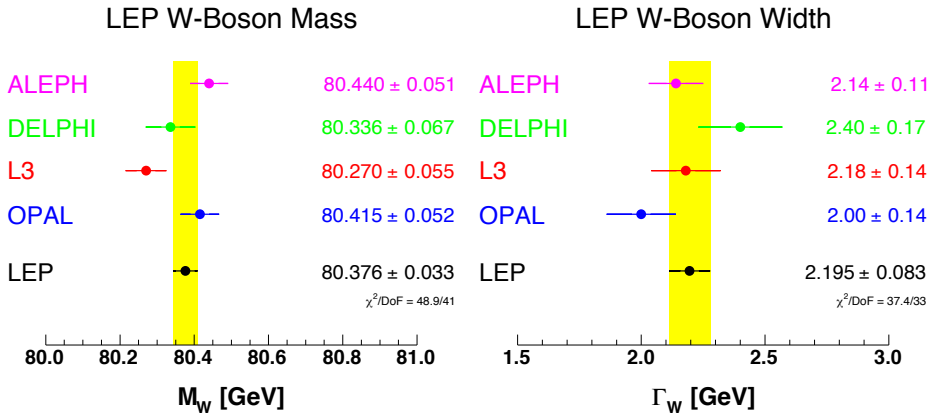

Fig. 3.5: Measurements of the W mass (left) and width (right) by the four LEP experiments and their combination, as obtained from the kinematics of W-pair decay products [24].

In the kinematic reconstruction of the W mass from W-pair decays the fully hadronic (qqqq) and semi-leptonic (qq$\ell\nu$) final states are exploited, making use of events with either four jets or two jets, one lepton and missing energy. In both cases the reconstructed W mass values are obtained by imposing the constraint that the total four momentum in the event should equal to the known initial centre-of-mass energy and zero momentum. The four momentum constraints (4C) are implemented by means of a kinematic fit where the measured parameters of the jets and leptons are adjusted, taking account of their measurement uncertainties in such a

way as to satisfy the constraints of energy and momentum conservation. The 4C implementation allows to overcome the limitations of jet energy resolution on the W mass reconstruction, and improve the mass resolution from around 10 GeV to around 2 GeV.

The kinematic fit of final states with four-momentum conservation constraints can also be applied to other diboson productions at $\sqrt{s} = 160 - 365$ GeV, like Z-pairs and Zγ events. In the case of Zγ final states, also known as radiative returns to the Z-peak, the fit can be shown to lead to a reconstructed Z boson mass as [42]

$$m_{\mathrm{Z}}^2 = s\frac{\beta_1 \sin\theta_1 + \beta_2 \sin\theta_2 - \beta_1\beta_2|\sin(\theta_1+\theta_2)|}{\beta_1 \sin\theta_1 + \beta_2 \sin\theta_2 + \beta_1\beta_2|\sin(\theta_1+\theta_2)|} \tag{3.19}$$

where $\theta_{1,2}$ and the angle of the two leptons or jets from the Z decay, with respect to the photon direction, and $\beta_{1,2}$ are the leptons or jets, The formula in Eq. 3.19 is based on fixing the jet directions and velocities to their measured values but rescaling their energies to conserve four-momentum, that follows closely what is done in a kinematic fit.

The formula in Eq. 3.19 also shows the direct interplay between the reconstructed Z mass and the center of mass energy ($E_{\mathrm{CM}}^2 = s$). In practice the Z mass is reconstructed primarily through the decay products direction and their velocities in the case of hadronic jets, while the energy scale is set by the known collision energy. The same happens with the 4C kinematic reconstruction of W-pairs, where again the energy scale of jets is given by E_{CM} and the angular openings of jets and leptons carry the primary information to determine the W mass, with the jets velocities as the further valuable ingredient.

On the other hand, in radiative returns, by making use of the value of m_{Z} precisely measured at the Z pole, the collision energy E_{CM} can be treated as the parameter to be measured in Eq. 3.19, so that the kinematic fit of radiative decays can be used to determine E_{CM}. This interpretation was used with LEP2 data to cross-check the E_{CM} values, and the results are shown in Fig. [**?**].

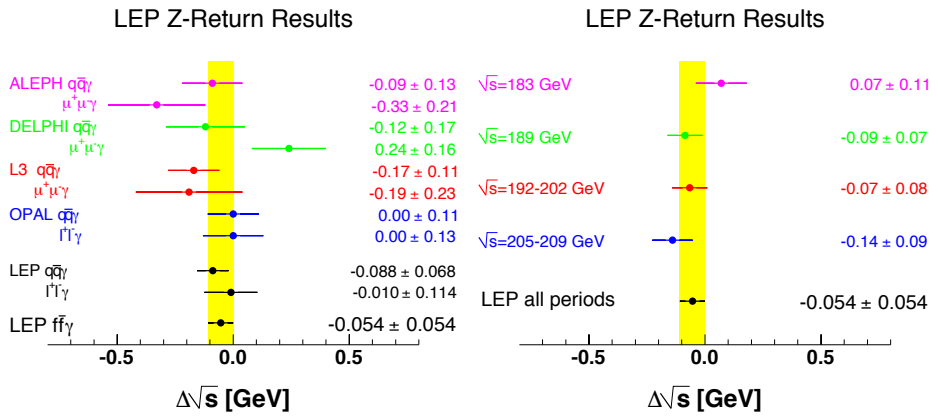

Fig. 3.6: Difference between the energy determined in Z-return events and the nominal LEP centre-of-mass energy, $\Delta\sqrt{s}$, for the different experiments and final states (left), and for the data taking periods with different energies (right) [24].

In general a 4C kinematic fit of either Zγ, ZZ, or WW decays can be equivalently employed to determine the boson (Z or W) mass, or the average center of mass energy.

More detailed studies on the FCCee specific prospects of W mass measurements from the kinematic reconstruction of W-pair decays are given in the following.

4.1 Simulation and reconstruction of the physics processes

The process $\mathrm{e^+e^-} \to \mathrm{W^+W^-}$ as well as the W pair decays were simulated with the event generator PYTHIA 8 [43]. Samples of 50k events were generated in both hadronic and semi-leptonic decay channels including initial and final states radiations (ISR and FSR). Colour reconnection were also included in the full hadronic decay. The Bose-Einstein final state interactions and the background processes were not included. The W mass and width were set to their PDG values, respectively 80.385 GeV/c^2 and 2.085 GeV/c^2. For the semi-leptonic decay, only the muon decay of the leptonic part has been studied.

The interaction of the decay products in the detector was done through the CLD-type detector using the PAPAS fast simulation and the HEPPY analysis framework [44] described in Section **??**. The particles were reconstructed with a particle flow algorithm, associating the tracks and the energy deposits in calorimeters. In the hadronic channel, all stable particles were forced into four jets using the ee-kt algorithm, also referred as the Durham algorithm [45]. To limit effects of bad clustering, events with at least one jet composed of single photon were rejected. In the semi-leptonic channel, the most energetic muon was identified as the leptonic W decay product. Each photon closer to the muon rather than any other particle or the beam axis and at least 0.4 radians away from other charged tracks was labelled FSR photon and combined with the lepton. The neutrino was associated with the missing momentum. All remaining particles were forced into two jets and clustered with the ee-kt algorithm (Durham).

PARAGRAPH ENERGY MEASUREMENT. DIFFERENT METHODS USED IN THE FOLLOWING PARAGRAPHS.

4.2 Energy rescaling

In the case of the hadronic channel, the method of energy rescaling can be used to correct for detector resolution and build a set of 4-vectors compatible with the energy-momentum conservation, i.e.,

$$\sum E = \sqrt{s} \quad and \quad \sum \vec{p} = \vec{0}$$

The jet energies are computed with the jet directions and velocities, $\beta_{jet} = E_{jet}/p_{jet}$, assuming that these quantities are exactly measured. By energy-momentum conservation, a solution to this problem can be found solving the system of linear equations (3.20) :

$$\begin{pmatrix} 1 & 1 & 1 & 1 \\ \beta_{x,1} & \beta_{x,2} & \beta_{x,3} & \beta_{x,4} \\ \beta_{y,1} & \beta_{y,2} & \beta_{y,3} & \beta_{y,4} \\ \beta_{z,1} & \beta_{z,2} & \beta_{z,3} & \beta_{z,4} \end{pmatrix} \begin{pmatrix} E_1 \\ E_2 \\ E_3 \\ E_4 \end{pmatrix} = \begin{pmatrix} \sqrt{s} \\ 0 \\ 0 \\ 0 \end{pmatrix} \tag{3.20}$$

Once the energies are computed, jets momentums are corrected with the rescaling factor α defined by the Equation (3.21), and the W mass is reconstructed with the new four-vectors.

$$\alpha = E_{computed}/E_{measured} \tag{3.21}$$

This method cannot be used in the semi-leptonic channel as the neutrino momentum is computed by energy-momentum conservation. The major disadvantage of this method is that the system (3.20) does not always have a physical solution. Frequently, the solution gives at least one zero or negative energy, in case of bad jet reconstruction due to high energy losses by ISR for instance.

4.3 Kinematic fit

The aim of the kinematic fit is to improve the resolution of a measured object slightly changing the measured quantities within their uncertainty to fulfil kinematics constraints. With n measured parameters $\vec{y}$, p unmeasured parameters $\vec{a}$ and m constraints $\vec{f}$, a kinematic fit will determine the corrections Δy to apply on parameters $\vec{y}$ such that :

- The weighted sum $\chi^2 = \Delta y^T V^{-1} \Delta y$ is minimal. V is the covariance matrix of the measured parameters. The resulting χ^2 can be interpreted as the probability of the proposed kinematic hypotheses to be true for the observed event.
- All constraints are fulfilled for parameters $\vec{a}$ and $\vec{y}$, i.e. $f_m(\vec{a}, \vec{y}) = 0$.

To solve this problem, the Lagrange Multipliers definition is used and the function to minimize is :

$$L = \Delta y^T \, V^{-1} \, \Delta y + 2 \sum_{i=1}^{4} \lambda_i f_i(y) \tag{3.22}$$

If the constraints are linear the solution is found in one step, otherwise, the constraints are linearised with a first-order Taylor expansion and the solution is found iteratively.

4.3.1 Hadronic channel

In the hadronic channel the final state is fully measured. Each of the jet four-vectors is expressed as a function of measured parameters which will be tuned to satisfy the fit constraints : the energy-momentum conservation (4C) with equality of the reconstructed W bosons masses (5C). The measured parameters used for the jet parametrization are the energy rescaling coefficients α – as defined by (3.21) –, the jet polar angles θ and ϕ and the jet velocities. The velocity is expressed as the logarithm of the boost $\log(\beta\gamma)$ to remove the limit $\beta < c$. As the parameters are non-linear, they are considered uncorrelated and then the covariance matrix can be assumed to be diagonal. The parameters uncertainties are obtained from the sigma of the Gaussian fits of the distributions of the difference between the reconstructed and generated jet energies, angles and velocities.

Since there are three possibilities to combine the four jets, the most likely jet pairing should be chosen. An approach is to repeat the fit for each different permutation. This method requires a long computation time and a great alternative is to select the pair minimizing the difference between the reconstructed invariant mass and the reference W mass, taken to be $80.385\ GeV/c^2$. With this method, the pairing efficiency is 97% at energy threshold and 99% at higher energy.

– –

Here : Distribution of the average of W mass for hadronic channel, compared to raw mass, simple rescaling for 161.6, 240 and 365 GeV + comments.

– –

4.3.2 Semi-leptonic channel

This decay channel is identified as two jets, a charged lepton and missing momentum tagged as the neutrino. The four-vectors of the jets are parametrized with the same measured parameters as in the hadronic channel. In the lepton parametrization only the energy is varied while other parameters are fixed. The neutrino is introduced in the fit as unmeasured parameter in the constraints. Two constraints were applied : the energy-momentum conservation (1C because of the neutrino) with equality of the reconstructed W bosons masses (2C).

– –

Here : Distribution of the average of W mass for semi-leptonic channel compared to raw mass for 161.6, 240 and 365 GeV + comments.

– –

4.4 Extraction of the W mass

The W boson mass is determined by comparison of the distribution with templates generated for $M_W \pm 1\ GeV/c^2$. The figure of merit (FOM), computed like a binned maximum likelihood, is used to estimate the statistical uncertainty on M_W. The expected statistical uncertainties on the W mass in hadronic (resp. semi-leptonic) decay channel for the different centre-of-mass energies planned at FCC-ee and for different reconstruction methods are gather in Table 3.2 (resp Table 3.3). The results are given for the full luminosity.

Table 3.2: Expected statistical uncertainties on W boson mass for the hadronic decay channel at FCC-ee with the CLD detector for different centre-of-mass energies and different reconstruction methods.

$\sqrt{s}\ [GeV/c^2]$	162.6	240	365
Luminosity (ab^{-1})	8	5	1.7
Raw Mass	value	value	value
Energy rescaling	value	value	value
4C fit	value	value	value
5C fit	value	value	value

Table 3.3: Expected statistical uncertainties (MeV/c^2) on the W boson mass for the semi-leptonic decay channel at FCC-ee with the CLD detector for different centre-of-mass energies and different reconstruction methods.

$\sqrt{s}\ [GeV/c^2]$	162.6	240	365
Luminosity (ab^{-1})	8	5	1.7
Raw Mass $[MeV/c^2]$	0.41	0.44	1.08
1C fit $[MeV/c^2]$	0.32	0.32	0.76
2C fit $[MeV/c^2]$	1.61	0.30	0.66

– –

Here : Comments. –

5 Cross section measurements

To be done by **Paolo**. *Check what is included already in previous sections*

The measurements of diboson total and differential cross sections with FCC-ee data will allow direct and indirect tests of the SM predictions. A more general exploration of all four-fermion final state productions will be crucial to acquire a finer knowledge of couplings, radiative corrections and the possible presence of new physics effects.

The W-pair cross section is defined with the CC03 component of four-fermion final state productions [24]. The measurement of the W-pair cross sections near the kinematic threshold has been discussed in Section 2 in the context of extracting precise values of the W mass and width. It was shown that if relevant systematic uncertainties on the event selection acceptance, efficiency, on the backgrounds, and on the integrated luminosities are kept to the required control levels, a statistical precision at the level of $2 \cdot 10^{-4}$ on the total cross section σ_{WW} can be achieved. A similar precision of $\sim 10^{-4}$ will be achievable also for σ_{WW} at higher centre of mass energies, where larger W-pair cross section values and lower backgrounds, will allow for a superior event selection quality.

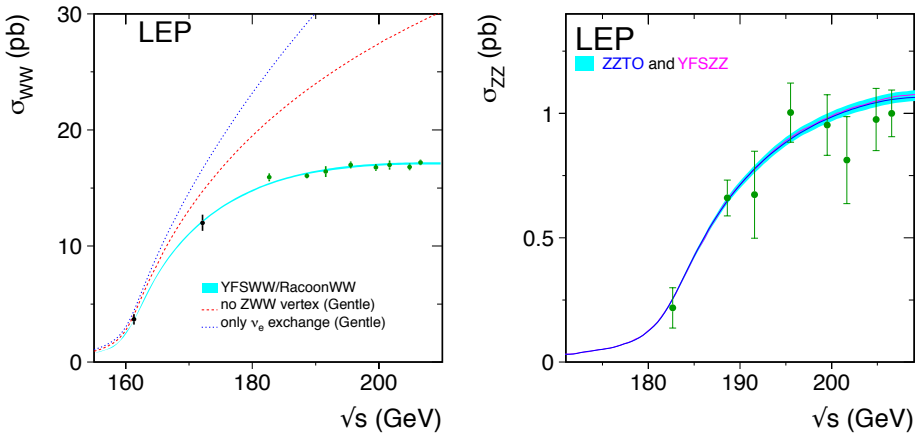

Fig. 3.7: Measurements of the total W-pair (left) and Z-pair (right) production cross sections as currently determined by LEP2 data [24]. Shaded areas represent uncertainties on the shown theoretical predictions, at the 2-0.4% level for W-pairs, and 2% for Z-pairs.

Figure 3.7 shows the W-pair cross sections as measured with LEP2 data as a function of the centre of mass energy from 161 GeV to 209 GeV. The uncertainties on the theory predictions shown in the plots are smaller but comparable to the experimental precision. Improved theory predictions have subsequently been produced [46], but further improvements will be necessary for the theory uncertainties to match the projected FCCee precision on this front. The $\sim 10^{-4}$ precision that will be achievable for σ_{WW} at the FCCee higher energies will be useful to verify the accuracy of theoretical radiative corrections, and can be exploited to obtain constraints on the theory fundamental parameters, like $\sin\theta_W$.

In analogy to W-pairs, the Z-pair cross section is defined with the NC02 component of four-fermion final state productions [24]. Figure 3.7 shows the Z-pair cross sections as measured with LEP2 data as a function of the centre of mass energy from 183 GeV to 209 GeV, results and theory predictions are in agreement with an overall experimental precision of 5% and

a theory prediction uncertainty of 2%. FCCee data will allow the measurement of Z-pair cross sections at 240 GeV and 365 GeV with a precision of 0.1%, and also in this case improved theory uncertainties will be needed to match the experimental precision. Precision measurements of the total and differential Z-pair cross sections will be essential to reach a fine knowledge of this process that will be a background to other FCCee measurements and searches. The Z-pair measurements will also be used to explore in depth new physics scenarios as the possible presence of neutral gauge self couplings.

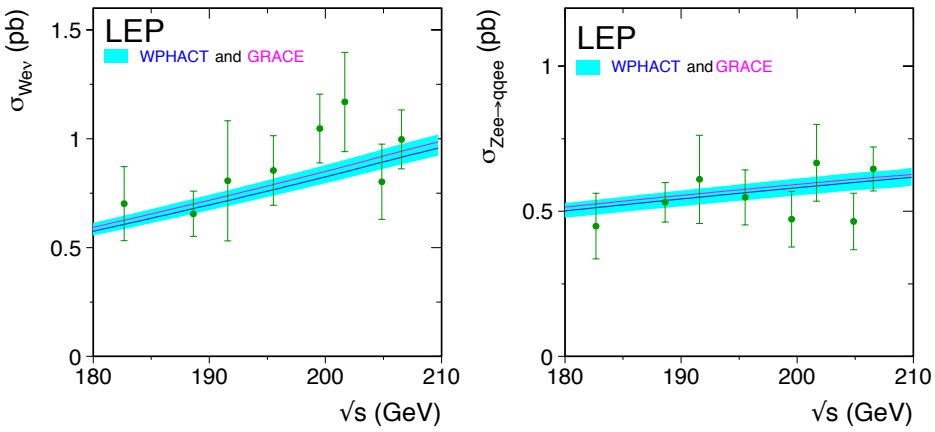

Fig. 3.8: Measurements of the total single-W (left) and single-Z (right) production cross sections as currently determined by LEP2 data [24]. Shaded areas represent 5% uncertainties on the shown theoretical predictions.

The Weν (single W) and Zee (single Z) processes have been defined with phase-space cuts on their four-fermion final states [24]. Results of measurements with LEP2 data are shown in Fig. 3.8. FCCee data will allow the measurement of single W and Z cross sections at 240 GeV and 365 GeV with a precision of 0.1%, and also in this case improved theory uncertainties will be needed to match the experimental precision. It will be important to achieve these precise determinations of the single-V processes, as they are backgrounds to the respective V-pair productions, and can interfere with those in the final states with electron decays. Total and differential cross sections will also serve to explore the structure of charged gauge couplings, with single-W events, and neutral gauge couplings with single-Z events.

A summary of diboson and single boson production cross section precisions obtained with LEP2 data, and achievable with FCCee data is given in Table 3.4.

Triple boson production measurements will also be accessible with FCCee.

The WWγ final states will be relatively abundant both at $\sqrt{s}$=240 and 365 GeV. With the LEP fiducial definition [24] the expected cross sections at FCCee will be around 0.3 pb, and relative precisions of some 0.1% can be obtained with the 240 GeV data. With this process total and differential cross sections will allow to explore the WW$\gamma\gamma$ and WWZγ quartic gauge couplings.

The production of three heavy weak bosons will only be accessible with the $\sqrt{s}$=365 GeV data, where cross sections of 10 fb and 0.5 fb are expected respectively for the WWZ and ZZZ final states [47]. These processes will therefore be measurable with precisions of 1-5%, and

Table 3.4: Relative precision on the determinations of the total W and Z pair and single productions. Final combined results with LEP2 data are compared to the projected precision obtainable with FCC-ee at different energy points.

Channel relative precision	WW	ZZ	Weν	Zee
LEP2 183-209 GeV	0.8%	5%	8%	6%
FCCee 162 GeV	$2{\cdot}10^{-4}$		$5{\cdot}10^{-4}$	$5{\cdot}10^{-4}$
FCCee 240 GeV	$1{\cdot}10^{-4}$	$5{\cdot}10^{-4}$	$5{\cdot}10^{-4}$	$1{\cdot}10^{-3}$
FCCee 365 GeV	$3{\cdot}10^{-4}$	$1{\cdot}10^{-3}$	$5{\cdot}10^{-4}$	$1{\cdot}10^{-3}$

$\sqrt{s}$	Luminosity	# of WW events
161 GeV	$10\,\mathrm{ab}^{-1}$	$\sim 3 \times 10^7$
240 GeV	$5\,\mathrm{ab}^{-1}$	$\sim 8 \times 10^7$
350 GeV	$0.2\,\mathrm{ab}^{-1}$	$\sim 0.2 \times 10^7$
365 GeV	$1.5\,\mathrm{ab}^{-1}$	$\sim 1.5 \times 10^7$

Table 3.5: A summary of the FCC-ee runs with the center of mass energy, integrated luminosity and the expected number of events for $e^+e^- \to WW$. The Z-pole run is below the WW threshold and is not included in this table.

constraints on the structure of WWZZ and WWZγ quartic gauge couplings will be derived.

6 Constraints on trilinear couplings

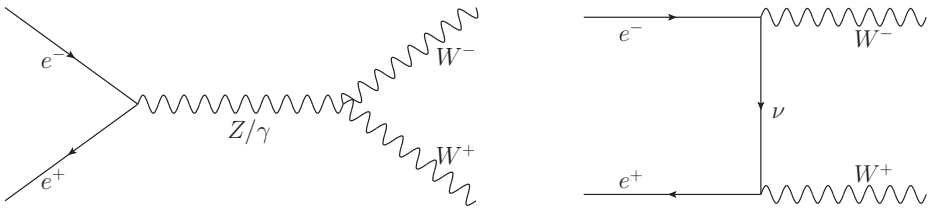

Fig. 3.9: The leading-order diagrams that contribute to $e^+e^- \to WW$. The s-channel diagram on the left with an intermediate Z or photon involves a triple gauge coupling.

The determination of the triple gauge couplings (TGC) has very important implications on beyond-standard-model (BSM) physics [48, 49]. At lepton colliders, the TGCs can be probed with the measurements of the diboson process, $e^+e^- \to WW$, shown in Figure 3.9. Such measurements have been performed at the LEP II run, with the triple gauge couplings being constrained to the level of a few percents [24]. The FCC-ee can measure the diboson process at several different energies with a much larger total luminosity, as summarized in Table 3.5. As such, it is expected to probe the TGCs with precision far better than the LEP ones. The study reported here aims to provide a simple estimation of the precision reaches on the TGCs at the FCC-ee.

A model-independent parameterization of the triple gauge couplings in the presence of BSM physics can be done in the effective-field-theory (EFT) framework, in which the Standard

Model Lagrangian is supplemented by higher dimensional operators. Imposing baryon and lepton numbers conservations, all higher dimensional operators are of even dimension. The theory at the electroweak scale can then be written as

$$\mathcal{L}_{\rm EFT} = \mathcal{L}_{\rm SM} + \sum_i \frac{c_i^{(6)}}{\Lambda^2}\mathcal{O}_i^{(6)} + \sum_j \frac{c_j^{(8)}}{\Lambda^4}\mathcal{O}_j^{(8)} + \cdots \tag{3.23}$$

If the scale of new physics Λ is sufficiently large, the leading effects of new physics at the electroweak scale are well parameterized by dimension-six operators. The CP-odd TGCs receive very strong constraints from electron EDM experiments, which are typically several orders of magnitude stronger than the collider bounds [50–52].

We therefore focus on the contributions of CP-even dimension-six operators, and the triple gauge couplings are given by [1]

$$\begin{aligned}
\mathcal{L}_{\rm tgc} \;=\;& ig s_{\theta_W} A^\mu (W^{-\nu} W^+_{\mu\nu} - W^{+\nu} W^-_{\mu\nu}) \\
&+ ig(1+\delta g_1^Z) c_{\theta_W} Z^\mu (W^{-\nu} W^+_{\mu\nu} - W^{+\nu} W^-_{\mu\nu}) \\
&+ ig\left[(1+\delta\kappa_Z) c_{\theta_W} Z^{\mu\nu} + (1+\delta\kappa_\gamma) s_{\theta_W} A^{\mu\nu}\right] W^-_\mu W^+_\nu \\
&+ \frac{ig}{m_W^2}(\lambda_Z c_{\theta_W} Z^{\mu\nu} + \lambda_\gamma s_{\theta_W} A^{\mu\nu}) W_v^{-\rho} W^+_{\rho\mu}\,,
\end{aligned} \tag{3.24}$$

where $V_{\mu\nu} \equiv \partial_\mu V_\nu - \partial_\nu V_\mu$ for $V = W^\pm,\, Z,\, A$.

Imposing gauge invariance, one obtains $\delta\kappa_Z = \delta g_{1,Z} - t^2_{\theta_W}\delta\kappa_\gamma$ and $\lambda_Z = \lambda_\gamma$. The contribution from new physics can thus be parameterized by 3 anomalous triple gauge couplings (aTGCs), $\delta g_{1,Z}$, $\delta\kappa_\gamma$ and λ_Z. In the effective-field-theory language, these three aTGCs correspond to three combinations of Wilson coefficients of the dimension-six operators which are independent of those that can be constrained by Z-pole measurements or the W mass. On the other hand, $\delta g_{1,Z}$ and $\delta\kappa_\gamma$ are generated by operators that also contribute to Higgs couplings, which leads to an interesting interplay between TGC and Higgs measurements [53]. Since the diboson process has a much larger cross section than the Higgs processes at the FCC-ee, it is expected that the TGC measurements can provide the best constraints on those operators and thus play a crucial role in probing Higgs related operators in a global framework [54–56].

The cross section of $e^+e^- \to WW$ at leading order is shown in Figure 3.10 as a function of the center of mass energy. While the WW threshold run has the largest luminosity, the cross section is suppressed by the phase space. Furthermore, near the threshold the amplitude of $e^+e^- \to WW$ is dominated by the t-channel diagram which does not contain the triple gauge vertex. As a result, the threshold run has little constraining power on the aTGCs. [2] The 350 GeV run has a small luminosity and a center of mass energy very close to 365 GeV. Indeed, while the diboson measurements could be done at four energies listed in Table 3.5, the most constraining power comes from the two runs at 240 GeV and 365 GeV. It is therefore necessary to exploit the angular distributions in order to simultaneously constrain all three aTGCs in a global analysis. In addition, the angular distributions of the diboson process can be particularly

[1] c_{θ_W} and s_{θ_W} are shorthands for $\cos\theta_W$ and $\sin\theta_W$, where θ_W is the weak mixing angle. θ_W is also used later to denote the production polar angle of $e^+e^- \to WW$. The definition should be clear from the context.

[2] This is verified by the results shown later in Table 3.7, as the addition of the threshold run provides almost no improvement on the top of the other runs.

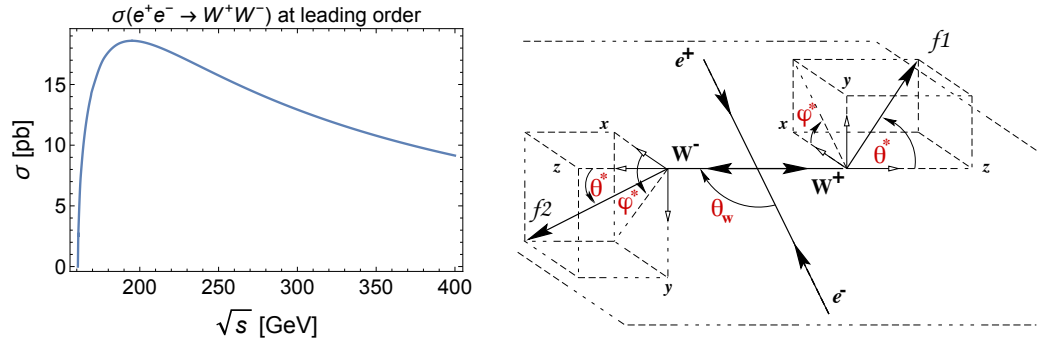

Fig. 3.10: **left:** The cross section of WW at leading order. **right:** The five angles in a WW event (taken from Ref. [57]), with the production polar angle θ_W.

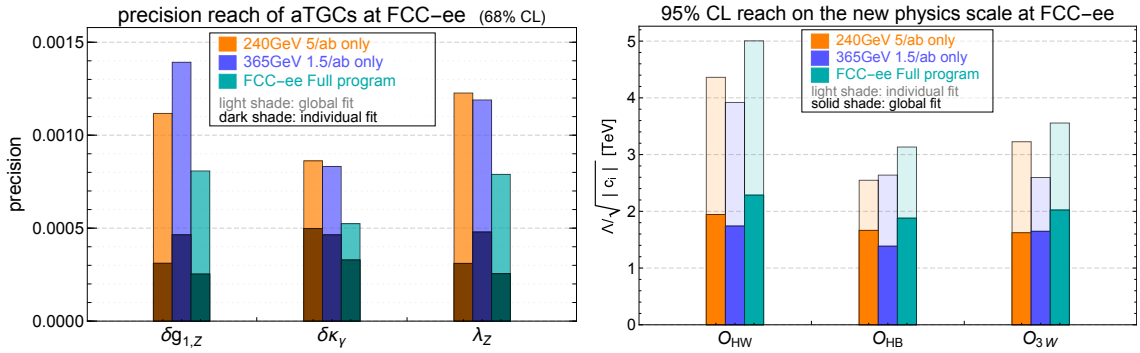

Fig. 3.11: **left:** The one-sigma precision reaches of the three aTGCs at the FCC-ee from the measurements of $e^+e^- \to WW$ in the semileptonic channel. We consider only the effects of signal statistics, assuming a 100% signal efficiency. **right:** The inferred 95% CL reaches on the new physics scale of the three dimension-six operators $\mathcal{O}_{HW}$, $\mathcal{O}_{HB}$ and $\mathcal{O}_{3W}$ defined in Table 3.6 with coefficients c_i/Λ^2.

helpful in probing the aTGCs due to the different helicity structures of the aTGCs and the standard model terms [58, 59].

The differential cross section of $e^+e^- \to WW$ can be parameterized by five angles – the production polar angle (θ_W) and two decay angles for each W, shown in Figure 3.10. A *chi-square* fit to the angular distributions is performed to estimate the precision reach of the three aTGCs at the FCC-ee. We use only the semileptonic channel, with one W decaying to e or μ and the other to jets. This channel has the advantages of both a sizable branching fraction ($\sim 29\%$) and easy event reconstruction. In particular, the neutrino can be reconstructed from the missing momentum, and the charges of the two Ws can be identified from the one of the lepton. The reconstructions of the hadronic W decay angles have ambiguities due to the challenges in discriminating q and $\bar{q}$ (and the corresponding angular distributions are "folded"), which are taken account of in the analysis. The distribution of each angle is divided into 20 bins. The *chi-square* is summed over all bins of the five angles, considering only statistical uncertainties of signal events.

We perform a simultaneous fit of all three aTGCs as well as individual fits of each aTGC assuming the other two are zero. The results are shown in the left panel of Figure 3.11.

Three scenarios are considered – the 240 GeV run only (orange), the 365 GeV run only

$\mathcal{O}_{HW} = ig(D^\mu H)^\dagger \sigma^a (D^\nu H) W^a_{\mu\nu}$	$\delta g_{1,Z} = -m_Z^2 \frac{c_{HW}}{\Lambda^2}$
$\mathcal{O}_{HB} = ig'(D^\mu H)^\dagger (D^\nu H) B_{\mu\nu}$	$\delta\kappa_\gamma = -m_W^2 (\frac{c_{HW}}{\Lambda^2} + \frac{c_{HB}}{\Lambda^2})$
$\mathcal{O}_{3W} = \frac{1}{3!} g \epsilon_{abc} W^{a\,\nu}_{\mu} W^b_{\nu\rho} W^{c\,\rho\mu}$	$\lambda_Z = -m_W^2 \frac{c_{3W}}{\Lambda^2}$

Table 3.6: The three operators corresponding to the aTGCs in a convenient basis (left) and the translation between the aTGCs and the Wilson coefficients (right).

(blue), and the full FCC-ee program (cyan) with WW measured at four different energies listed in Table 3.5. The one-sigma precisions (corresponding to 68% CL) from both the global fit and the individual fits are shown for the three aTGCs.

One important observation in Figure 3.11 is that the reaches of the 240 and 365 GeV runs are comparable.

This is because the sensitivities of the aTGCs grow with energy, and the the smaller statistics of the 365 GeV run is compensated by the larger sensitivities. A combination of the two runs thus further improves the precision reach of the aTGCs. The numerical results are also presented in Table 3.7 along with the correlations among the three aTGCs.

Assuming the Z-pole observables and the W mass are constrained very well, the three anomalous couplings can be mapped to the three operators shown in Table 3.6 in a convenient basis [55, 60]. [3]

The precision of the aTGCs are then translated to the reach on $\Lambda/\sqrt{|c_i|}$ in the right panel of Figure 3.11 for the three operators, where Λ is the scale of new physics and c_i the coupling of the operator, as defined in Equation 3.23. If the couplings are naïvely assumed to be of order one ($c_i \sim 1$), the TGC measurements at the FCC-ee are sensitive to new physics scales at multiple TeVs.

It should be noted that, with the one-sigma bounds of the three aTGCs and the correlation matrix in Table 3.7, the likelihood of the TGC measurements can be reconstructed, which can used to obtain the results in any other basis or derive the constraints on any particular model that predicts non-zero aTGCs.

In a combined analysis of the four experiments at LEP [24], the aTGCs are determined to be $\delta g_{1,Z} = -0.016^{+0.018}_{-0.020}$, $\delta\kappa_\gamma = -0.018 \pm 0.042$ and $\lambda_Z = -0.022 \pm 0.019$ at 68% CL, each obtained by an individual fit with the other two set to zero. While the global-fit results are not available in the combined analysis, they are reported in the ALEPH analysis [62] to be $\delta g_{1,Z} = 0.042^{+0.036}_{-0.048} \pm 0.013$, $\delta\kappa_\gamma = -0.049^{+0.060}_{-0.047} \pm 0.030$ and $\lambda_Z = -0.040^{+0.036}_{-0.036} \pm 0.011$, with the first (second) error bar being the statistical (systmatic) uncertainty. The reaches of aTGCs at the FCC-ee are thus at least one order of magnitude better than the LEP ones. We illustrate this in Figure 3.12, where the FCC-ee reaches are compared with the LEP ones.

Since the aTGCs have sensitivities that grow with energy, the LHC could potentially provide competitive reaches on them by exploiting differential cross sections at high invariant mass [63]. However, the validity of the EFT framework could become questionable at very high energies, creating potential issues in the interpretation of the results [64, 65]. In addition, the bounds on aTGCs are usually derived under the assumption that new physics affects the diboson process only at the triple gauge vertex. This "TGC dominance" assumption may not be well justified for the LHC measurements [66]. High energy linear colliders may also face

[3] A more general parameterization of the aTGCs can be found in Ref. [61].

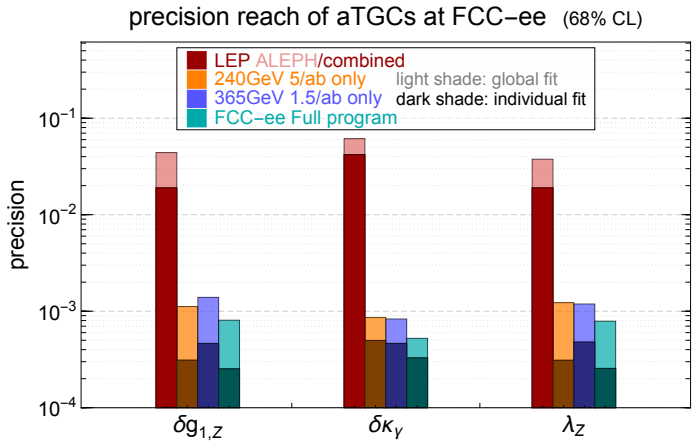

Fig. 3.12: The one-sigma precision reaches of the three aTGCs at the FCC-ee from the measurements of $e^+e^- \to WW$ in the semileptonic channel shown in log scale. The LEP reaches are also shown for comparison. The LEP results of individual fits are taken from the combined analysis [24], while the global ones are taken from the ALEPH paper [62]. For illustration, the central values of the LEP results are not shown, and the precision are averaged over the positive and negative one-sigma bounds if they are asymmetric.

FCC-ee $e^+e^- \to WW$ semileptonic channel all angles								
	240 GeV only				**365 GeV only**			
	uncertainty	correlation matrix			uncertainty	correlation matrix		
		$\delta g_{1,Z}$	$\delta\kappa_\gamma$	λ_Z		$\delta g_{1,Z}$	$\delta\kappa_\gamma$	λ_Z
$\delta g_{1,Z}$	11.2×10^{-4}	1	0.08	-0.90	13.9×10^{-4}	1	-0.57	-0.80
$\delta\kappa_\gamma$	8.6×10^{-4}		1	-0.42	8.3×10^{-4}		1	0.10
λ_Z	12.3×10^{-4}			1	11.9×10^{-4}			1
	240/350/365 GeV				**161/240/350/365 GeV**			
	uncertainty	correlation matrix			uncertainty	correlation matrix		
		$\delta g_{1,Z}$	$\delta\kappa_\gamma$	λ_Z		$\delta g_{1,Z}$	$\delta\kappa_\gamma$	λ_Z
$\delta g_{1,Z}$	8.1×10^{-4}	1	-0.28	-0.87	8.1×10^{-4}	1	-0.28	-0.87
$\delta\kappa_\gamma$	5.2×10^{-4}		1	-0.12	5.2×10^{-4}		1	-0.12
λ_Z	7.9×10^{-4}			1	7.9×10^{-4}			1

Table 3.7: The one-sigma precision reaches from a global fit of the three aTGCs at the FCC-ee and the correlations among them. Four scenarios are considered, which are the 240 GeV run only, the 365 GeV run only, the combination of the 240, 350 and 365 GeV runs and the full FCC-ee scenario (with the addition of the threshold run).

similar problems in probing the aTGCs. The FCC-ee, on the other hand, has the advantage that the diboson process is measured at relative lower energies with much better precisions, which ensures that the EFT expansion in Equation 3.23 is valid. The Z-pole run at the FCC-ee also sets very strong constraints on the non-aTGC contributions to the diboson process, providing very good justifications to the "TGC dominance" assumption that we made.

This is a simple study, under ideal assumptions, to estimate the precision reach of the three aTGCs at the FCC-ee. A more realistic analysis needs to be done in the future to study

the impact of backgrounds, detector resolutions, selection efficiencies, and other possible effects. The hadronic and dileptonic decay channels, while facing more challenges in the event reconstructions, should be included to further improve the sensitivity to the aTGCs. One may also try to optimize the statistical methods in order to extract all possible information from the measurements.

7 Performance requirements for diboson physics

To be done by **Paolo**.

7.1 Detector performance requirements

7.2 Specific requirements on the accelerator